5-2016

Coercivity Enhancement and Gamma Phase Avoidance of Alnico Alloys

Li Zhang

University of Nebraska-Lincoln, lizhang129@hotmail.com

Coercivity Enhancement and Gamma Phase Avoidance of Alnico Alloys

by

Li Zhang

A THESIS

Presented to the Faculty of

The Graduate College at the University of Nebraska

In Partial Fulfillment of Requirements

For the Degree of Master of Science

Major: Mechanical Engineering and Applied Mechanics

Under the Supervision of Professor Jeffrey E. Shield

Lincoln, Nebraska

May, 2016

Coercivity Enhancement and Gamma Phase Avoidance of Alnico Alloys

Li Zhang, M.S.

University of Nebraska, 2016

Advisor: Jeffrey E. Shield

The promotion of social progress requires greater levels of energy efficiency,
quality and productivity. However, these developments usually come at the cost of the
environment. Green technologies such as electric vehicles, wind turbine and solar panels
are ironically overshadowed by supply limitations and high prices of rare earth elements.
Therefore, it is important to find alternative materials to replace those that contain critical
elements. Alnico alloys show high magnetization, high Curie temperature (800°C) and
good corrosion resistance, making it one of the best candidates to replace
neodymium-based magnets used in electric vehicles.

In this thesis, methods controlling shape anisotropy and grain microstructure
were used to improve magnetic properties of Alnico. For shape anisotropy, we studied the
effects of isothermal heat treatment (IHT), secondary annealing (SA), and alloy
composition. The magnetic properties of Alnico were found to be highly sensitive to IHT
temperature and time rather than SA temperature and time. Since shape anisotropy is
driven by microstructure evolution, it is likely that the evolution has mainly been
determined by IHT processing. We found Co increases the spinodal decomposition
temperature while it is decreased by Ti. For grain microstructure, we tuned it by
controlling wheel speed, and found the optimal magnetic properties were obtained at 20

mps. Textured Alnico was fabricated by setting up a simple casting system. However, a steep temperature gradient was unstable during the casting process due to heat transfer into the atmosphere.

The non-magnetic gamma (γ) phase is known for its deleterious effect on the magnetic properties of Alnico. Here, alloying additions of Sn and Ge were found to decrease amount of γ phase. The role of Sn or Ge could be to suppress γ phase formation or shrink the temperature range over which the γ phase is stable. Furthermore, we studied the effect of magnetic field annealing, and found that its effectiveness depends on IHT temperature and alloy composition. For Alnico 9, the maximum coercivity of 1416 Oe can be obtained after full heat treatment.

Acknowledgements

Firstly, I would like to appreciate Dr. Jeffrey Shield for being my advisor. While working with him at such a flexible environment, not only I have learned how to play well with alloys and magnets, but also found the beauty of them. He revealed a beautiful metallurgical world to me. In this world, I attempted to apprehend structural beauty under the bottom, and figure out what do atoms think.Those precious experiences inspired me to become an engineer who are willing to make a difference for our world.

I would also like to thank Dr. QingxiuJia and Dr. Qiang Chen who introduced me to materials research during college and pulled me back from fashion design. Without their help I may not even get closer to materials.

I would like to thank Dr. Wenyong Zhang for his continuous guidance, encouragement and criticism on research projects, which allowed me to become proficient with magnetic characterization and analysis.

I would like to thank the committee members: Dr. Bai Cui, Dr. Eli Sutter for their time and advice on my thesis.

I would like to thank Dr.David Sellmyer for his collaboration and access to his lab for magnetic heat treatment and measurements. I would also like to thank Dr. Shah Valloppilly, Dr. Steven Michalski, Dr. Lanping Yue, Dr. Wen Qian, Dr. Xingzhong Li and Bhaskar Das for their training and assistance with NCMN and NERCF facilities.

I would like to thank our research group members that I have worked with: Meiyu Wang, Mak Koten, Edwin Peng, James Doyle, Mike Lucis, Yunlong Geng. A special thanks to Mak Koten and Edwin Peng for their valuable comments on my thesis.

Sometimes, the most important decisions in our life are made by an emotional rather than intellectual process, if the choice "feels right" is usually taken. But people I encountered along the way and intensively personal experiences influenced my choice. Last but not least, I would like to thank those people for enriching my life.

"Carpe diem. Seize the day, boys. Make your lives extraodinary."

-Dead Poets Society, 1989

Table of Contents

List of Figures

List of Tables

Chapter 1 Introduction

1.1 Permanent Magnets

Permanent magnets are ferromagnetic materials that keep their magnetism in the absence of magnetic field. The oldest known permanent magnet is lodestone, which is a naturally magnetized mineral magnetite (Fe_3O_4) with inclusions of maghemite (cubic Fe_2O_3)[1]. According to the 5th century BC book of *the Guanzi*[2] and the 2nd century BC chronicle *the LüshiChunqiu*[3], people found some magic stones that attract iron. They called these stones *Ci Shi*, which means love stones. Ancient people regarded the attraction as the love from parents to their children. They thought the stones were parents of iron, and only loving parents can attract their children[4]. The first recorded magnetic device is called *Si Nan*, which means "pointing to the south"[5][6]. It is a spoon-shaped compass made of lodestone. When "the spoon" stopped rotating, the spoon handle points to the south, while the head of the spoon points to the north. Figure 1 shows modern duplicated *Si Nan* maded by technology historian Zhenduo Wang[7]. Although there is a doubt about whether *Si Nan is* a compass made of lodestone[8], it is believed that medieval Chinese navigators were using lodestone compasses by the 12th century[1].

Figure 1.Modern duplicated Si Nan model.

The modern permanent magnets history started in the beginning of twentieth century, while high carbon steels and then tungsten or chromium steels replaced lodestone acting as the best available permanent magnet[9].

In 1940s, Tokushichi Mishima of Japan discovered Alnico alloys[10][11]. A family of Fe-based alloys with primary addition of Al, Ni and Co, and minor addition of Cu and Ti. Alnico has relatively high coercivity (up to 2000 Oe for Alnico 8H) and good thermal stability (around 800 °C), and the best reported energy product exceeding 10 MGOe (79.6 KJ/m^3) for Alnico 9[12]. Generally, there are two ways to make Alnico magnets, they can either be cast or sintered[13].

In 1966, the magnetic properties of YCo_5 phase was discovered, followed by $SmCo_5$. The combination of rear earth elements (REEs) and transition metals (TMs) has great potential for permanent magnets because REEs are known for their high anisotropy and

TMs usually have high magnetization and Curie temperature. The magnetic properties of

SmCo-type permanent magnet were improved with the development of Sm_2Co_{17} in 1976.

Its maximum energy product is over 30 MGOe (240 kJm^{-3})[9].

General Motors in the USA and Sumitomo Special Metals of Japan simultaneously

discovered the magnetic properties of $Nd_2Fe_{14}B$ in 1984[9] by different processing routes.

General Motors used melt spinning to make ribbon-like raw materials. After melt

spinning, there are three different methods to make commercial products. Ribbons can be

blended with resin to make bonded permanent magnets. They can also be hot pressed to

improve density, which gives a higher energy product. Furthermore, they can be die upset

to make dense anisotropic permanent magnet, and maximum energy products of 50

MGOe (400 kJm^{-3}) can be achieved due to crystallographic alignment.

Sumitomo Special Metals invented a powder metallurgy processing route. In their

methods, an as-cast ingot is broken into powder by exposing to hydrogen.This process is

called hydrogen decrepitation (HD). The size of HD powder is further reduced by a jet

milling.When a fine size is achieved, each particle of powder is single crystalline,which

can then be aligned well in magnetic field. After alignment, the compact is heated in

vacuum to remove hydrogen. Finally, the magnets are quenched and heat treated to get

optimal magnetic properties.

Permanent magnets have a big impact on our daily life. Generally speaking,

applications of permanent magnets can be divided into four categories as follows[14]:

(1) Using tractive or repelling force of the magnet to do mechanical work, such as

magnetic separators or magnetic holding devices.

(2) Using the energy stored in a ferromagnetic material and the principle of Lenz's Law to convert mechanical energy into electrical energy, such as in generators or wind turbines.

(3) Using the energy stored in a ferromagnetic material and the principle of Lenz's Law to convert electrical energy into mechanical energy, such as in motors or loudspeakers.

(4) Using the magnetic field to direct, shape and control electron or ion beams, such as in ion pumps or cyclotrons.
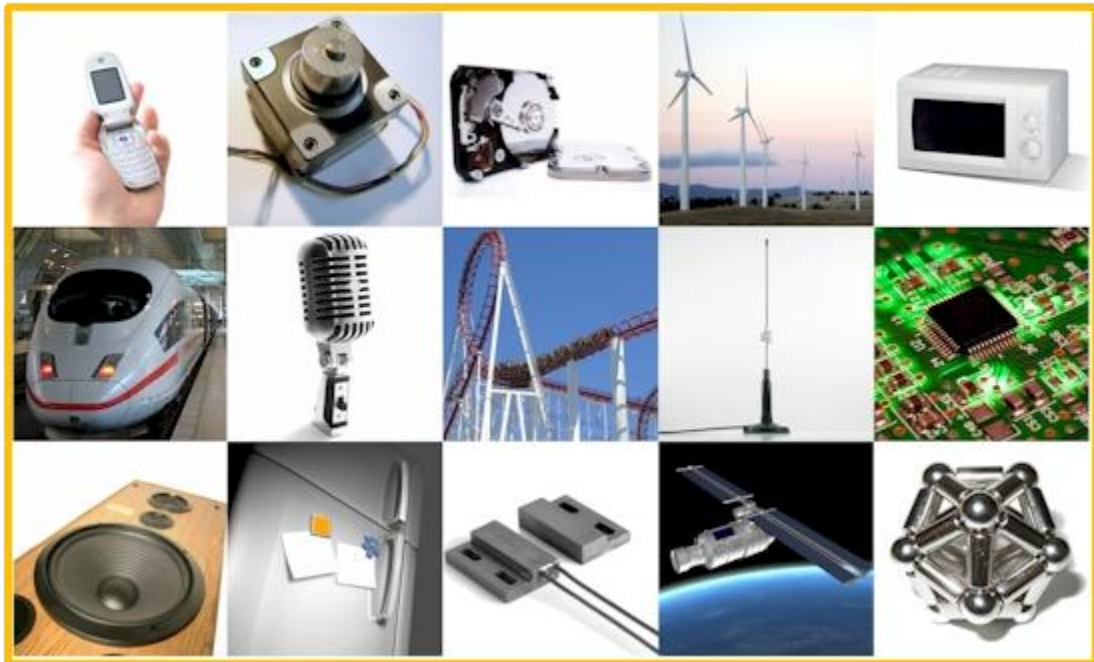
Figure 2.Diverse applications of permanent magnets[14].

1.2 Motivation

At the end of 2015, the leaders from more than 190 nations attended a summit in Paris that was aimed at preventing dangerous climate change[15]. At the meeting, the United States pledged to cut its greenhouse gas emission by 26-28% by 2025. This will require a multitude of changes to meet this goal. According to a new report from energy and environmental groups[16], electrification of 53% of the vehicle, along with more wind and solar power plants, the nation would reduce greenhouse gases of 550 metric tons per year in 35 years. This equals to 100 million gasoline and diesel vehicles taken off the road[16], which will help the nation to achieve the goal.

Electric vehicles and hybrid vehicles rely heavily on REEs. It is said each of the vehicle need 60 pounds of REEs[17]. Figure 3 shows the REES in the Toyota Prius. The vehicle occupys over 50% of the hybrid market in the United States, and has been called the biggest user of rare earths of any object around the world[17]. As we can see, REEs play a vital role in hybrid and electric vehicles. Neodymium magnets are important in electric motor and regenerative braking systems. Terbium and Dysprosium are added in neodymium magnets to improve their termal stability. All hybrid and electric vehicles on road rely heavily on lanthanum in battery pack[18]. Catalytic converters require cerium for the oxidation of CO and NO_x emissions in exhaust gases[19]. Currently, California is dedicated to 1.5 million electric cars on the road by 2025[16]. This transportation evolution will result in a potential demand of over 40 million kilograms of REEs in the

next few years.
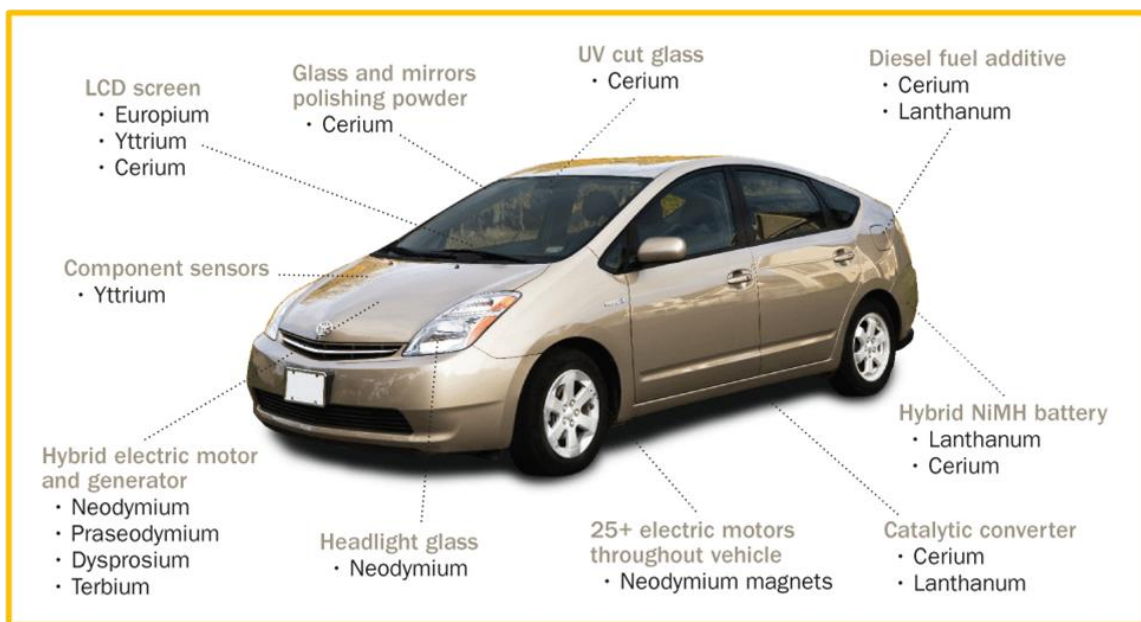
Figure 3.The REEs in Toyota Prius[17].

Rare earth elements are also essential for many other applications, such as compact fluorencent lamps, hard disk drives and other technical areas[20]. The versatility of REEs has given them technological, environmental, and economic importance.

However, REEs are naturally abundant in China, which controls about 95% of global rare earth production, and holds half the world's reserves of these metals[21]. Recently, in order to boost its own industry and prevent depletion of natural resources, China reduced its export quota, leading to high prices and supply chain disruptions around the globe[21].

Therefore, it is highly desirable to design and synthesize high energy product permanent magnets without REEs to compete with rare earth magnets and to achieve long term supply and cost outlook. One successful candidate is Alnico, due to its cost

efficiency, relatively good magnetic properties, and high working temperature. This will enable domestic automobile makers to provide a broad range of vehicles with electric drive motors[22].

1.3 Objective

Our study aims to optimize the thermal treatment processing and composition of Alnico alloys. Different solidification rate of melt-spun Alnico ribbons created different grain features compared with cast and sintered Alnico. The investigation of the relationship between grain microstructure and magnetic properties are important for coercivity enhancement, since the methods to improve the coercivity of Alnico is deficient. A non-magnetic (gamma) phase in Alnico is detrimental to its magnetic properties, therefore, it is necessary to develop methods to get rid of it.

Specifically, the objectives of our research are as follows:

(1) To study the effect of heat treatment and composition on magnetic properties of melt-spun Alnico alloys;

(2) To investigate the effect of solidification process on the grain microstructural and magnetic properties of melt-spun and cast Alnico alloys;

(3) To discovery new alloying elements that could be effective to remove gamma phase.

Chapter 2 Literature Review

2.1 History of Alnico Alloys

Alnico permanent magnets were developed in early 1930s by Japanese scientist Tokushichi Mishima[10][11]. He developed permanent magnet made from nickel, aluminum and iron with better magnetic properties than "magnet steels" available at the time. A few months later, he reported addition of cobalt (Co) could further enhance the magnetic properties of the alloy[23].

In 1935, researcher William E.Ruder of General Electric developed a new Alnico permanent magnet. An Alnico disk of less than a pound can be used to swing a 55-lb.radio cabinet. This suggested that Alnico was ready to replace small electromagnets in motors, transformers, and loudspeakers, which show great potentials in lowering the cost and simplifying the construction[24].

Anisotropic Alnico alloys with columnar grains were developed by Gottfried Bruno Jonas of the Netherlands in late 1930s. Such alloys show 50% to 200% higher maximum energy product than isotropic Alnico[24]. Since that time, Alnico had been developed into a robust permanent magnet. However, commercial exploitation of this material was stopped by the advent of World War II. It was not until 1947 that Alnico speakers was used in guitar amps of Gibson and Fender[24], which indicated the rise of Alnico products. Figure 4 shows an advertisement from QST amateur radio magazine released in

April 1945, exhibiting importance of Alnico.

Since researchers cannot further improve the remanence of Alnico, they switched their attention to coercivity enhancement. Koch *et al.* found Ti-containing Alnico has better coercivity, followed by the development of Alnico 8[25]. However, Ti introduces grain refinement, which makes it difficult to obtain a columnar structure. At that time, there was considerable doubt in the Alnico industry that any practical results could be achieved[26].

Figure 4. An advertisement from QST amateur radio magazine (April 1945)[24].

In the early of 1960s, Gould discovered that appropriate sulfur (S) addition to Alnico

8 produced columnar crystals without sacrificing large magnetic properties[27][28].

Since then, further work on composition modification to improve coercivity without

reducing remanence led to the introduction of Alnico 9 in the U.S. market in 1964[26].

Research on Alnico stopped after 1975, after the emergence of high coercivity rare

earth permanent magnets, such as samarium cobalt and neodymium iron boron. There has

been no significant progress on magnetic properties of Alnico since 1964, as can be seen

in Figure 5. Today, researchers are focusing on understanding coercivity

mechanisms[29][30], microstructure[31], and processing[31][32] to improve its magnetic

properties.
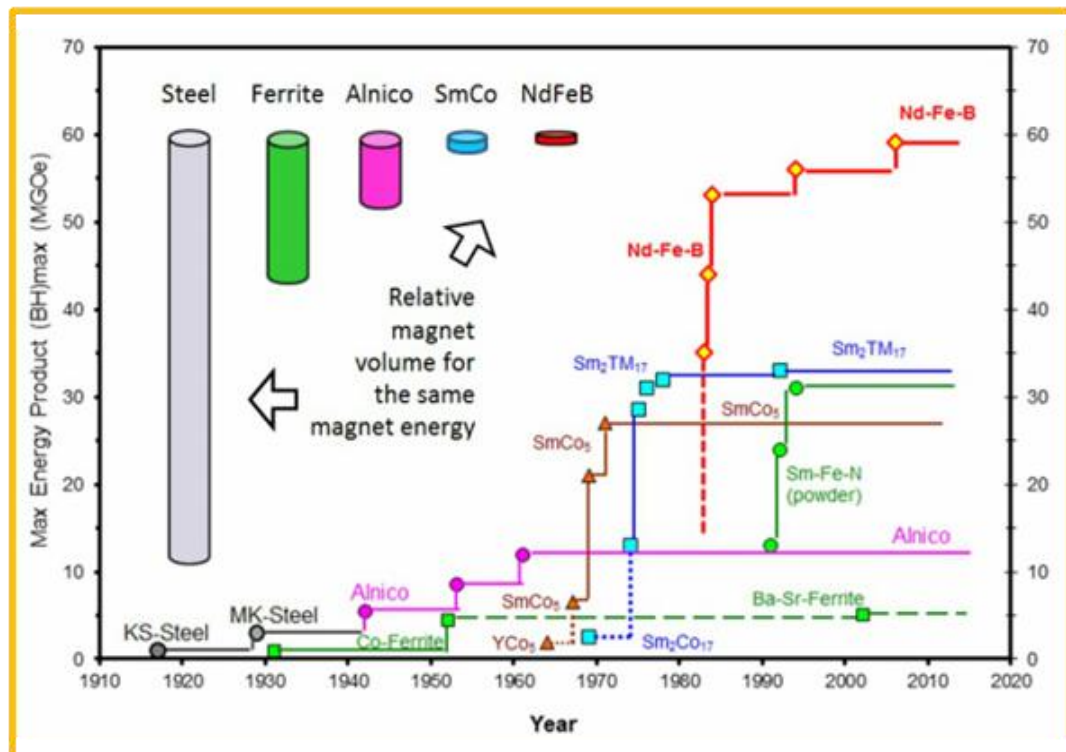
Figure 5. Permanent Magnets History in the Aspect of Magnet Energy[33].

2.2 Magnetic origin of Alnico Alloys

Magnetic properties of Alnico results from the phase transformation (spinodal decomposition). α_1 (Fe-Co rich) and α_2 (Al-Ni rich) phases are developed in Alnico after spinodal decomposition, in which α_1 phase is strong ferromagnetic, while α_2 is weakly ferromagnetic. α_1 phase is aligned as rods in <100> direction and distributed in α_2 phase, since <100> is the energetically favorable direction[34].

Spinodal decomposition is a continuous phase transformation arising from conserved order parameter, which means it cannot change in one location without affecting its neighborhood[35]. As can be seen in Figure 6, an alloy with composition X_0 is heat treated at T_1 and then quenched to T_2, Its composition is homogeneous and initial free energy is G_0 at the beginning. However, the alloy will be immediately unstable due to small variations in composition, producing A-rich and B-rich phase will reduce the total free energy. Therefore, 'up-hill' diffusion occurs until the equilibrium composition X_1 and X_2 are achieved[36]. There is no activation energy barrier inside the spinodal area. If the alloy lies outside the spinodal area, small fluctuation of composition results in free energy increase, and the alloy is metastable. In order to reduce the free energy of the system, nucleation and growth will take place. Therefore, 'down-hill' diffusion occurs in this situation, as can be seen in Figure 7.

There are three high-energy Alnico alloys, which are Alnico 5, Alnico 8, and Alnico 9. Figure 8 shows magnetic properties of these three Alnico grades. Alnico 5 has the highest remanence compared to other two grades. However, Alnico 8 has the maximum coercivity. Alnico 9 combines characteristics of Alnico 5 and Alnico 8, showing the maximum energy product. The difference of magnetic properties among these Alnico alloys results from various chemical composition, followed by shape anisotropy variation.
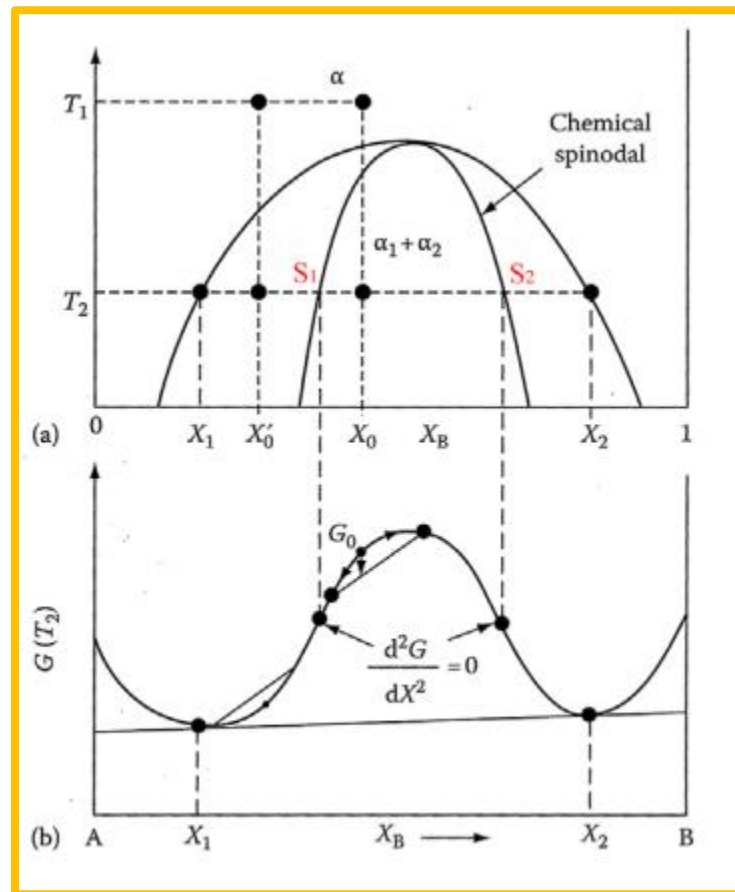
Figure 6. Phase diagram and free energy curve of spinodal decomposition[36]**.**
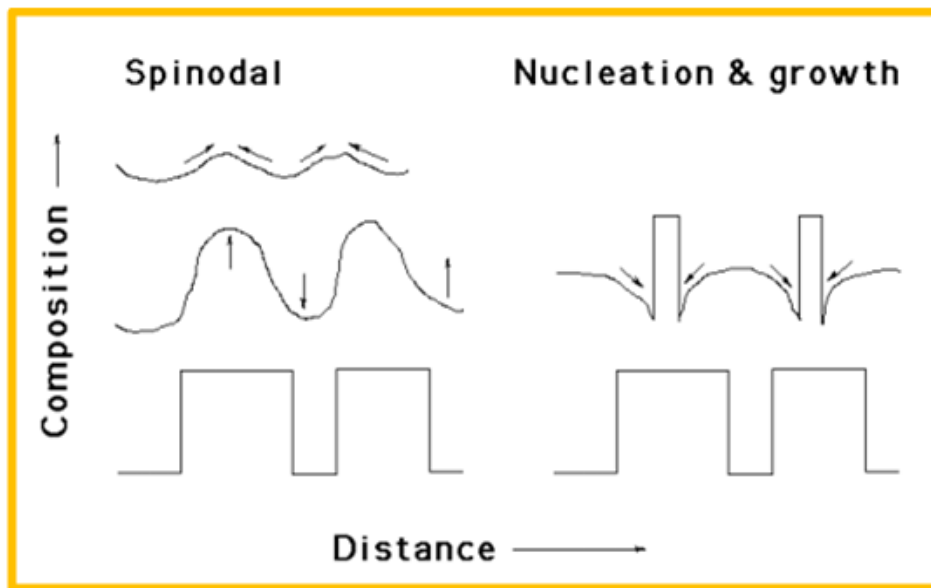
**Figure 7. Composition profiles of spinodal decomposition and nuleation&
growth**[36]**.**
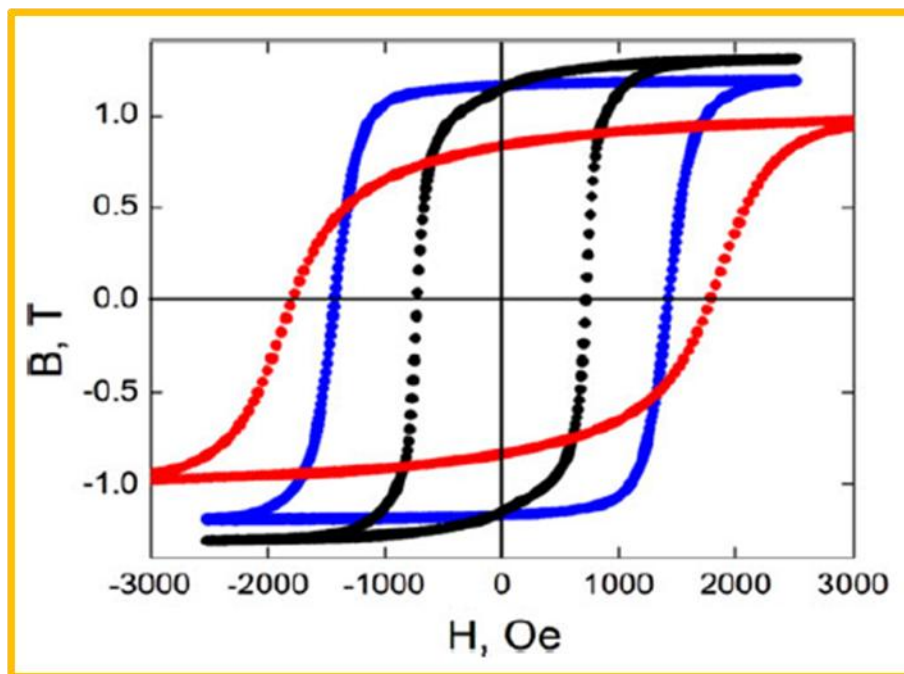
**Figure 8. Magnetic hysteresis loop of three high-energy Alnico grades: Alnico 5
(black), Alnico 8 (red) and Alnico 9 (blue). The higher B_r for the Alnico 5 and 9 are
consistent with their high grain alignment relative to the applied field direction
during processing compared to Alnico 8, which has randomly oriented grains[29].**

The coercivity of Alnico is largely determined by shape anisotropy[37][30]. Figure 9

shows high-angle-annular-dark-field (HAADF) scanning transmission electron (STEM)

imaging, which clearly differentiates phase morphology in Alnico alloys[30]. The aspect

ratio of α_1 phase in Alnico 5 is about 5, however, Alnico 8 and Alnico 9 has larger aspect

ratio, which is around 10.

$$H_{ci} = (1 - \rho)(N_b - N_a)C^{Fe+Co}M_s^{Fe,Co} \tag{1}$$

where ρ is volume fraction of α_1 phase, N_b is demagnetizing factor along the long axis,

N_a is demagnetizing factor along the short axis, C^{Fe+Co} is the relative concentration of

Fe+Co in the α_1 phase, $M_s^{Fe,Co}$ is saturation magnetization of the sample.

Equation (1) [30] shows that the intrinsic coercivity of Alnico alloys is proportional

to the difference in the demagnetizaing factor between the long axis and the short axis.

Therefore, a high aspect ratio of α_1 phase is beneficial for coercivity improvement. This

characteristic is used to design high coercivity Alnico alloys.
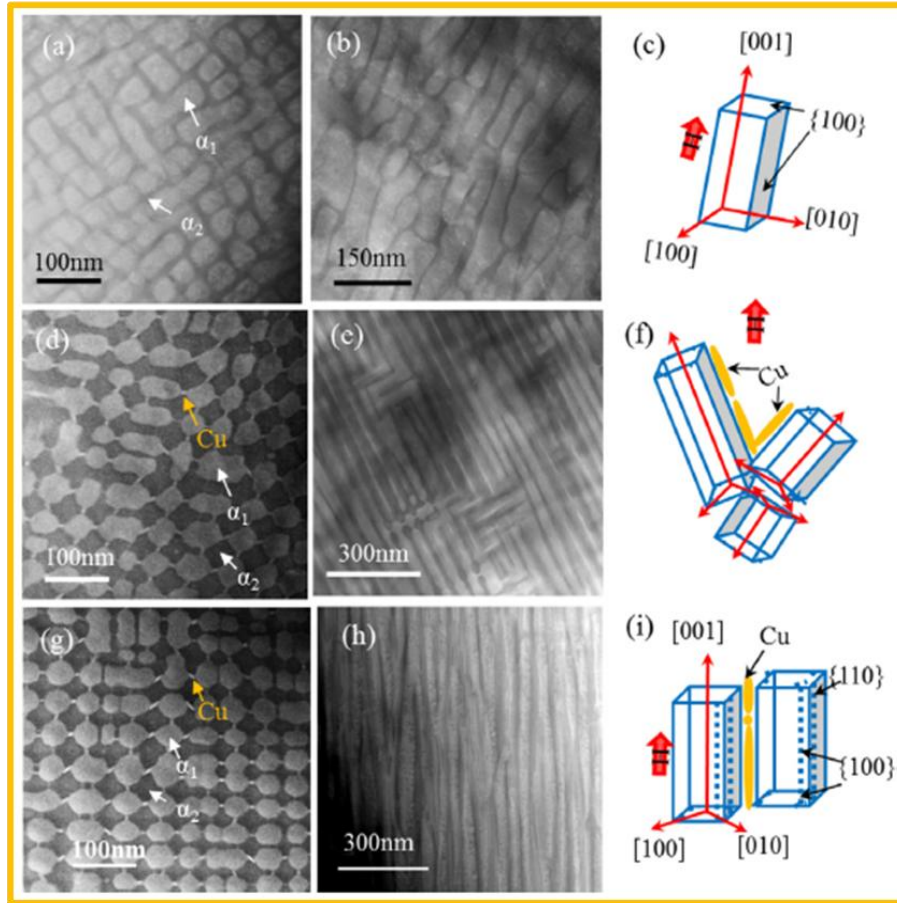
Figure 9. HAADF STEM images and schematic of α_1 phase morphology of different Alnico alloys: (a) Alnico 5,transverse; (b) Alnico5, longitudinal; (c) model of α_1 phase in Alnico 5; (d) Alnico 8, transverse; (e) Alnico 8, longitudinal; (f) model of α_1 phase in Alnico 8; (g) Alnico 9, transverse; (h) Alnico 9, longitudinal; (i) model of α_1 phase in Alnico 9[30].

2.3 Manufacturing Process

Commercial Alnico alloys are fabricated by casting and sintering. For castAlnico, pure elements are put into a furnace and melted at 1750-1780 °C. The molten Alnico alloy is poured into sand molds with required shape of magnet. The sand mold and casting is cooled rapidly to avoid the formation of gamma phase. Sometimes there are chilled plates at the bottom of the molds to aid cooling. Sand can be exothermic sand,

which gives a different cooling rate. Exothermic sand is combined with chilled plates to produce textured Alnico alloys with higher remanence values. After cooling, the sand mold is broken down and the magnets retrieved. A series of heat treatments are applied to as-casted Alnico. If required, the magnets are ground to finished size and are also magnetized before packing[13].

Sintered Alnico is made by compacting powder. Firstly, the raw elements are ground by milling into particles. Secondly, the powder is pressed in a die under tonnes of pressure. The resulting magnet is then sintered at 1260 °C in a hydrogen atmosphere to melt the powder together. Generally, sintered Alnico magnets are small, weighing less than 30 grams[13].

2.4 Heat Treatment

As-made Alnico alloys are magnetically soft, with the coercivity of a few oersted. Their relatively good magnetic properties are given by heat treatment. Therefore, heat treatment study is very important for improving Alnico alloys' performance. Heat treatment of Alnico alloys depends on their types. Typically, the heat treatment of Alnico includes three steps. For Alnico 5, samples are heat treated at 1350 °C to reach the single phase, and then are fast cooled to 900 °C. This process is called solutionization, which is used to make homogeneous α phase and remove γ phase formed in Alnico preparation process. Samples are then cooled to 600 °C under a magnetic field where spinodal decomposition takes place. Following a double tempering for 6 hours at 650 °C and 24

hours at 550 °C to achieve chemical equilibrium between α_1 and α_2 phases[38]. For

Alnico 8 and Alnico 9, firstly, as made Alnico alloys are solutionalized above 1250 °C for

half an hour, and then are quenched to room temperature to achieve single phase.

Secondly, the quenched samples are annealed for 10 minutes at 800 °C in the presence of

a magnetic field for spinodal decomposition development[39]. The magnetic properties of

Alnico alloys are mainly determined in this process. Field annealing samples are

successively annealed at 650 °C and 550 °C as Alnico5, to sharpen phase separation,

followed by magnetic properties improvement.

Kim *et al.* reported the effect of cooling rate and low temperature solutionlization on

the magnetic properties of Alnico 5[40]. They found the magnetic properties of Alnico 5

are highly dependent on the cooling rate from 900 °C to 600 °C. The faster the cooling

rate is, the smaller the size and the larger aspect ratio of α_1 phase it will have, resulting in

better coercivity, as shown in Figure 10.

Iwama *et al.* studied the effect of isothermal annealing temperature on evolution of

phases, as can be seen in Figure 11. The quenched specimens were isothermally annealed

at 750, 780, 810, and 830 °C, respectively, with a magnetic field applied along the

columnar axis of the specimen. It shows α_1 phases aligned along the magnetic field

direction, and 810 °C producing the optimal morphology[34].
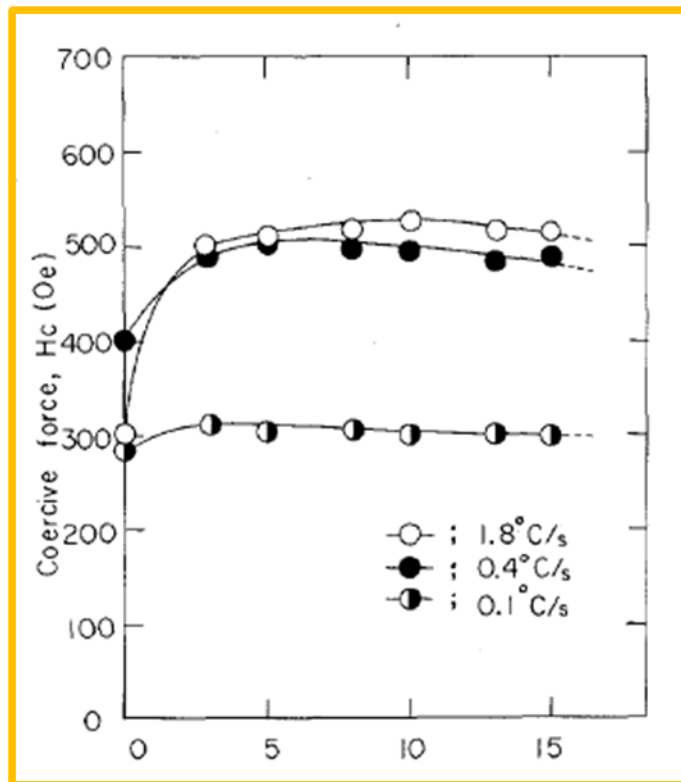
**Figure 10. Relation between coercive force and aging time at 600 °C for the
Fe-24Co-14Ni-8Al-3Cu alloy after continuous cooling in magnetic field from 900 °C
to 600 °C at various cooling rates. Solution treatment was performed at 1250 °C for
1h**[40]**.**
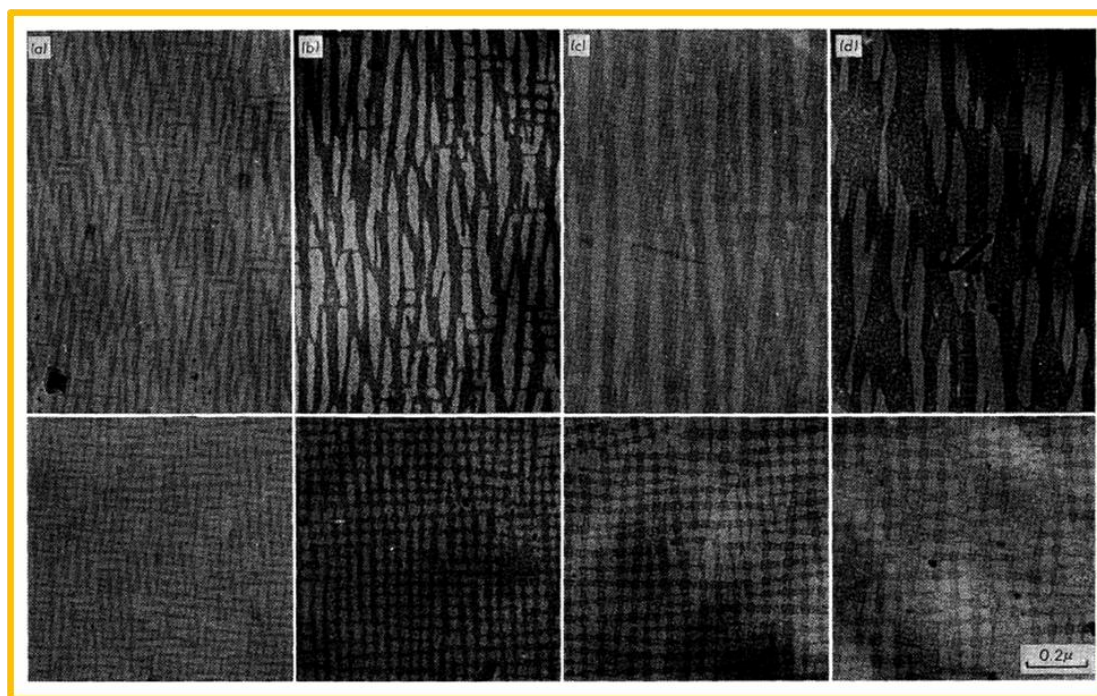
Figure 11. Electron micrographs of Alnico 8 specimens annealed for 10 minutes in a magnetic field at (a) 750 °C, (b) 780 °C, (c) 810 °C and (d) 830 °C, respectively. The upper row corresponds to the specimen surface parallel to the applied field and the lower row corresponds to the surface perpendicular to the field[34]**.**

2.5 Gamma Phase and Alpha Sub Gamma Phase

Gamma (γ) phase is an FCC phase which is notorious for its deleterious effect on the magnetic properties of Alnico alloys. The reason why it kills coercivity is not well understood. It is possible that the γ phase is a non-ferromagnetic phase whose existence destroys saturation magnetization and coervicity of Alnico. γ phase tends to form along grain boundaries[41]. Its stable region depends on alloy composition.The lowest solutionization temperature where γ phase can still be found increases with cobalt and decreases with titanium content[42]. In order to avoid γ phase, Alnico alloys can be heated to 1200°C to 1300 °C, held for 30 minutes or longer, and then quenched to bypass γ phase formation region[43][44][34]. However, when Co concentration is larger than 36 wt%, it is difficult to solutionize Alnico alloys without destroying previous grain microstructure, because the lowest temperature where γ phase formation does not occur nearly coincides with the solidus[42].

While cooling, γ phase diffusionlessly transforms to a BCC alpha sub gamma (α_γ) phase. Jullen*et al.*[45]studied its detrimental effect on magnetic properties of Alnico 8. They found remanence (B_r) was reduced markedly with increasing α_γ. The intrinsic coercivity is decreased about 18 Oe/% α_γ. Energy product ((BH)$_{max}$) is similar to B_r,

although it changes more drastically than B_r, as can be seen in Figure 12.
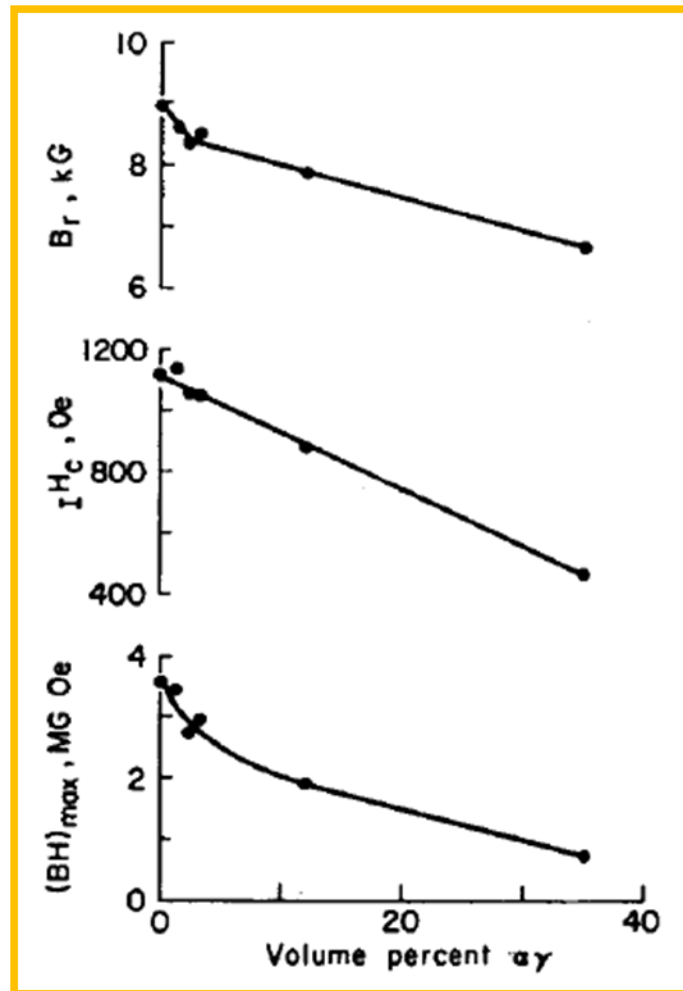
Figure 12. The effect of α_γ on magnetic properties of Alnico 8[45].

2.6 Alloy Addition

Alloy additions are an effective way to improve magnetic properties of Alnico alloys by controlling shape anisotropy and microstructures.The alloying elements for Alnico can be separated into two categories: (1) Elements that are used to boost intrinsic coercivity

of Alnico, and (2) elements to help columnar grain growth.

2.6.1 Coercivity Enhancers

Most of Co goes to α_1 phase after spinodal decomposition, which increases

saturation magnetization, resulting in higher B_r. Equation 2 shows this also enlarges the

magnetization difference between α_1 and α_2. H_c results from magnetostatic interactions,

as can be seen in equation 3[46]. Therefore, the coercivity of Alnico is increased with Co

addition. Here ΔM is the difference in saturation magnetization, $M_{\alpha 1}$ the saturation

magnetization of α_1 phase, $M_{\alpha 2}$ the saturation magnetization of α_2 phase, N_2 the

demagnetizing factor along the long axis, and N_1 the demagnetizing factor along the short

axis.

$$\Delta M = M_{\alpha 1} - M_{\alpha 2} \tag{2}$$

$$H_c \propto \Delta M(N_2 - N_1) \tag{3}$$

Liu *et al.* investigated Alnico alloys containing 34, 36, 38, and 40 wt% Co[47]. They

found that there was more α_1 phases with diameter smaller than 10nm when increasing

Co and Ti content in the samples, as can be seen in Figure 13.The coercivity largely

increases with Co, while the remanence and squareness of the demagnetization curve

decrease with Co. They explained that the increasing nonmagnetic Ti content is the

reason for saturation magnetization reduction. However, there is no report of Ti content

of their specimens. It is possible that particle alignment and perfection deteriorate with

Co, following with the reduction in saturation magnetization.

Table 1. Magnetic properties of Alnico 8[47]**.**

Alnico 8 (mass%) Co	B_r (T)	H_{cj} (kA/m)	$(BH)_{max}$ (kJ/m^3)	Hk/Hcj
34Co	1.14	117	93.5	0.89
36Co	1.13	126	104.3	0.88
38Co	1.08	132	97.9	0.85
40Co	1.04	144	93.4	0.83
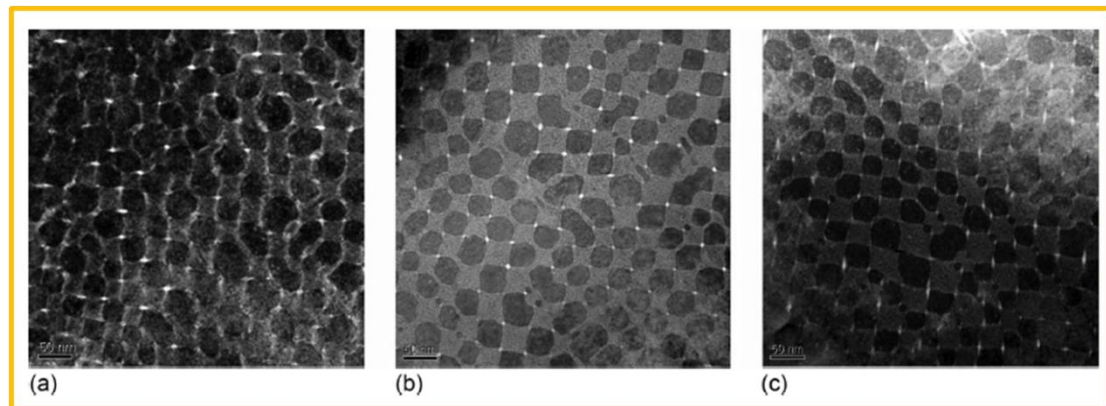
Figure 13. TEM of Alnico 8 thin foils perpendicular to the applied magnetic field. (a) bright-field image of 34 wt% Co Alnico; (b)36 wt% Co Alnico;(c) 40 wt% Co Alnico[47]**.**

Ti is another element that can boost coercivity of Alnico alloys. Alnico 8 and Alnico 9 are well-known due to their relatively high coercivity compared with Alnico 5, especially when an isothermal field treatment is applied[48]. Coercivity enhancement can be explained by the equation 2 and 3. Ti is a paramagnetic element, which primarily segregates to the α_2 phase[30]. This can increase the saturation magnetization difference between α_1 and α_2 phases, enhancing coercivity. Another reason is that Ti improves the shape anisotropy of Alnico alloys. This is proved by comparison of the aspect ratio of

Alnico 5, Alnico 8 and Alnico 9[30]. Alnico 5 usually has an aspect ratio of 5, while Alnico 8 and Alnico 9 have aspect ratiosof 10.

Takeuchi *et al.* performed anisotropy measurements using a combination of magnetic measurements and electron microscopy on monocrystallline Alnico alloys[49]. They found that the shape anisotropy constant increases with Ti content, resulting in coercivity improvement.They also found that the packing fraction of the α_1 phase dramatically changes with Ti, leading to the conclusion that one main reason for high coercivity of the high Ti-containing Alnico is the packing fraction. However, this finding does not agree with other work[30], which shows packing fraction has no obvious change among Alnico 5, Alnico 8, and Alnico 9.

Iwama *et al.* studied the effect of Ti in Alnico 8-type alloys[48]. Figure 14 shows that extrinsic coercivity ($_BH_c$) significantly increases as Ti content increases. It approaches 1700 Oe at 6 wt% Ti, and then slightly decreases. At the same time, B_r linearly decreases with Ti. The optimal Ti content is 5 wt%, which shows the highest $(BH)_{max}$. The electron microscopy images in Figure 15 reveal the precipitates particles after optimal heat treatment are likely to coarsen in both size and aspect ratio with increasing Ti. This finding seems to contradict the recent characterization study of Alnico 5, Alnico 8, and Alnico 9[30], and the later report about the effect of Ti on shape anisotropy[49]. It is likely that shape anisotropy is mainly determined by the synergy of Co and Ti, rather than by Ti itself, since Ti was increased while Co was deceased. On the contrary, high Ti-containing Alnico alloys usually have high Co content, which leads to improvement in

shape anisotropy and magnetic properties[30][49].
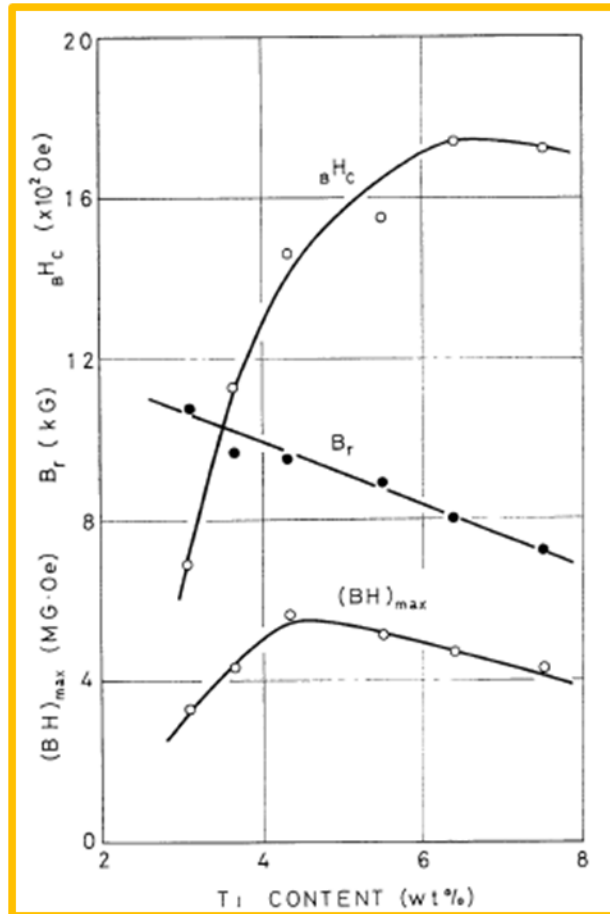
Figure 14. Relation between magnetic properties and Ti content in Alnico 8-type alloys under the optimal isothermal heat treatment[48]**.**
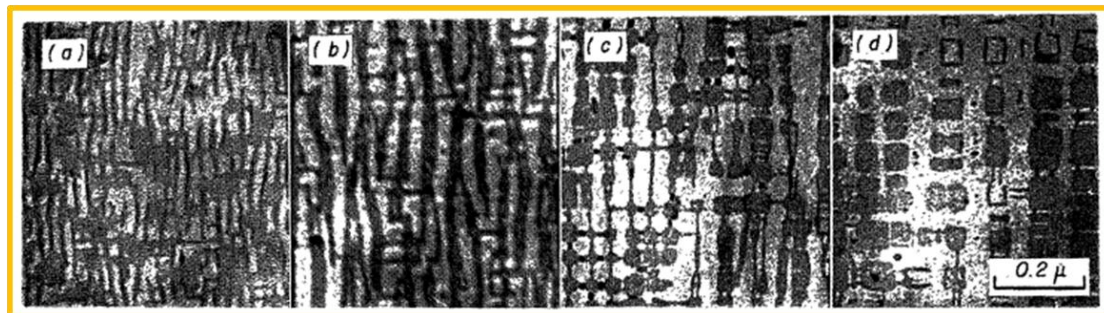
Figure 15. Electron micrographs of Alnico 8-type alloys containing various Ti content, after the optimal isothermal treatment followed by aging[48]**.**

(a)No.3 (3.10 wt% Ti) (b) No.5 (4.36 wt% Ti) (c) No.7 (6.39 wt% Ti) (d) No.8 (7.52

wt% Ti)

Nb is another element that can be used to enhance coercivity. The reason for

coercivity enhancement results from shape anisotropy improvement[50]. Although the

effect of Nb on the microstructure of Alnico alloys has not be studied, it is suggested that

it is similar to Ti addition[50]. Szymura *et al.* investigated the influence of Nb addition on

the magnetic properties of textured Alnico 5 alloy. They found 0.5 wt% Nb addition

decrease remanent induction while increasing coercivity and squareness of the hysteresis

loop[50]. Sugiyama *et al.* studied the effect of Nb on the magnetic properties of sintered

Alnico 5 alloys[51]. As can be seen in Figure 16, coercivity increases as Nb increases.

However, remanence gradually decreases when Nb addition is over 1%. They also

reported large amount of Nb addition cause pore aggregation, rapid grain growth, and

negative effects on rupture strength. They suggested that 0.35~0.70 wt% of Nb addition is

optimal to improve sinterd Alnico 5 alloys.
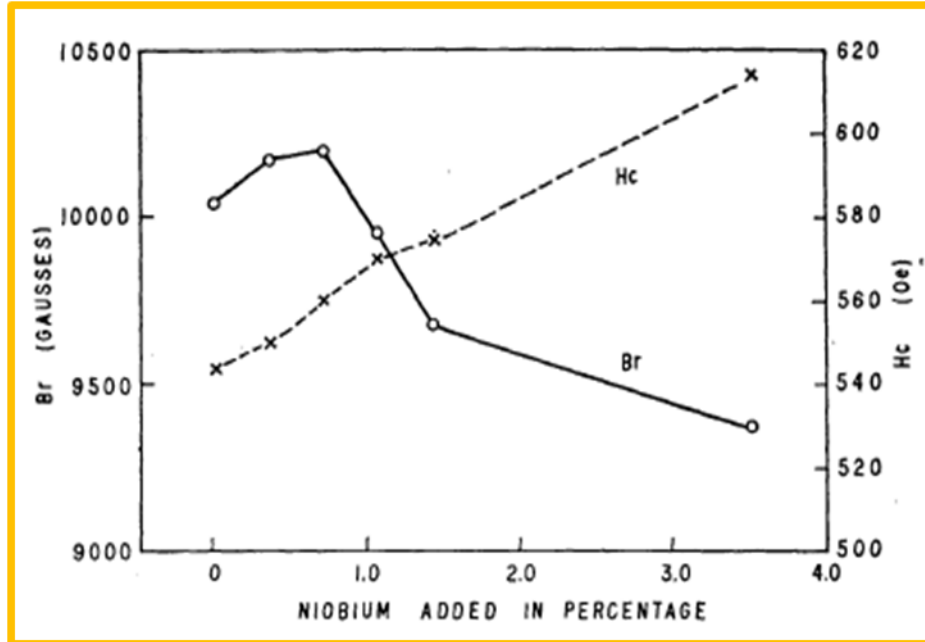
Figure 16. Effect of added Niobium on the magetic properties of sintered Alnico 5 magnet alloys[51]**.**

2.6.2 Crystallographic Texture Enhancers

Grains with preferential orientation create crystallographic texture[52].

Crystallographic texture strongly affects the shape of the hysteresis loop, making it more

square, resulting in magnetic properties improvement. As can be seen in Table 2, the

magnetic properties of Alnico are significantly improved with grain alignment. Therefore,

it is desirable to develop Alnico with crystallographic texture.

Table 2.Composition and magnetic properties of anisotropic, thermomagnetically treated Alnico 5 and 8 as well as single crystal Alnico 5.

Alnico	Character	Composition (wt%) (balance Fe)					Magnetic Properties		
		Ni	Al	Co	Cu	Other	B_r (T)	$_BH_c$ (kA/m)	$(BH)_{max}$ (kJ/m^3)
5	Random grain	12–15	7.8–8.5	23–35	2–4	0–0.5 Ti 0–1 Nb	1.2–1.3	52–46	40–44
DG^a 5	Directed grain 5	13–15	7.8–8.5	24–25	2–4	0–1 Nb	1.3–1.4	62–56	56–64
5 xtl	Single crystal	14	8	25	3		1.4	68	80
8	Random grain	14–15	7–8	37–40	3	7–8 Ti	0.74–0.78	150–170	44–48
DG 8(9)	Directed grain 8	14–16	7–8	32–36	4	0.3S	1.0–1.1	140–110	60–75

Alnico alloys containing Ti are especially attractive due to their high coercivity. However, it is very difficult to cast magnets with a columnar structure with Ti content higher than 0.7 wt%[53][54]. There are two explanations for grain refinement of Ti addition. Thomas *et al*. concluded that equiaxed grains formed at high Ti addition are caused by the combination of Al and Ti rather than Ti alone[55]. The addition of Al and Ti may widen solidus-liquidus gap, which creates a large concentration gradient in the liquid during solidification, followed by equiaxded grain formation. In contrast, Luteijin *et al.* suggested that titanium oxide, carbide and nitride after Ti addition act as heterogeneous nucleation sites, leading to grain refinement[56].

In order to obtain textured Alnico alloys when Ti is added, researchers searched for alloying elements that are beneficial for columnar grain formation. It was found that appropriate addition of S[53][57], Si[57], Se[53], Te[53], and C[53], or the combination thereof[54] help columnar grain growth without sacrificing magnetic properties. Makino

et al. reported textured Alnico 8 alloys can be prepared with 0.15 to 1.0 wt% S

addition[57].Columnar grains were easily obtained with increasing S content; however, S

can decrease magnetic properties. The optimal S addition is suggested take in the range of

0.15 to 0.3wt%.

They also studied the duplex effect of S and Te, which is more effective than adding

one element alone[54]. As can be seen in Figure 17, columnar grains of Alnico alloys

with 8.5 wt% Ti content can be obtained by duplex addition of S and Te.

Si is another texture enhancer. It is reported that by adding up to 1 wt% Si, magnetic

properties are equal to or better than Alnico 5 without Si addition[57]. Si lowers freezing

temperature, which results in a larger temperature gradient for solidification. This could

be beneficial for columnar grain growth.
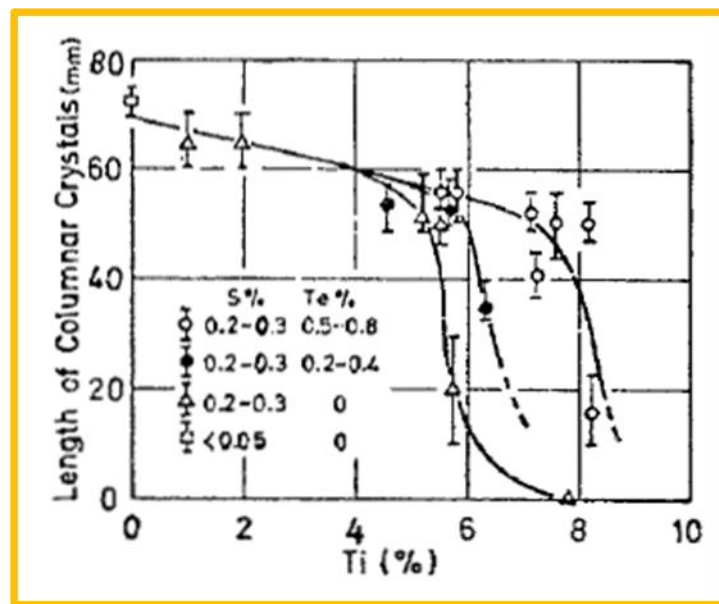
Figure 17. Effect of Ti contents on length of columnar crystals in Alnico magnet alloys[54]**.**

Chapter 3 Experimental Procedure

3.1 Arc Melting

Arc melting or vacuum arc melting is a traditional method used to prepare solid metal ingots. In our process, pure metals were placed on a water cooled copper plate. The chamber of the arc melter was repeatedly pumped and backfilled with high purity argon gas. The base pressure was around 100 mTorr and the operating temperature was slightly below atmospheric pressure. A large voltage was applied to tungsten electrode to generate the arc. Pure metals were melted by the arc with melting temperature up to 3500 °C and then formed a solid sample. The sample was then flipped and re-melted for four times to ensure chemical homogeneity.
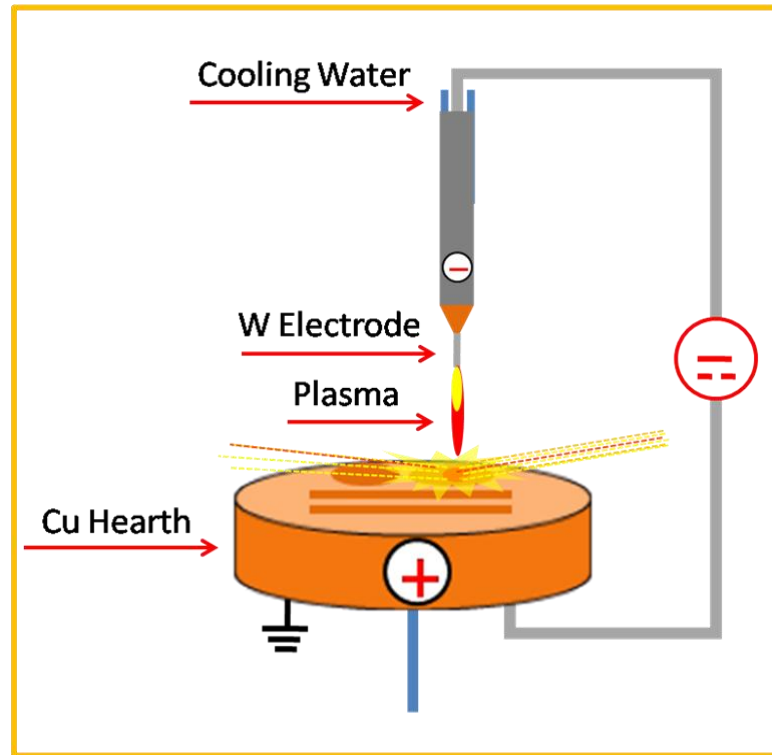
Figure 18.Schematic diagram of arc melter.

3.2 Melt Spinning

Melt spinning is a method that can control solidification and structure of

materials[58]. In our experiment, the base pressure was 2.3×10^{-2} Torr. Samples were

melted by radio frequency induction heat copper coil, and then ejected by over pressured

argon through a small round nozzle (0.72 mm in diameter) onto the rotating copper wheel.

Alnico ribbons were collected for characterization.
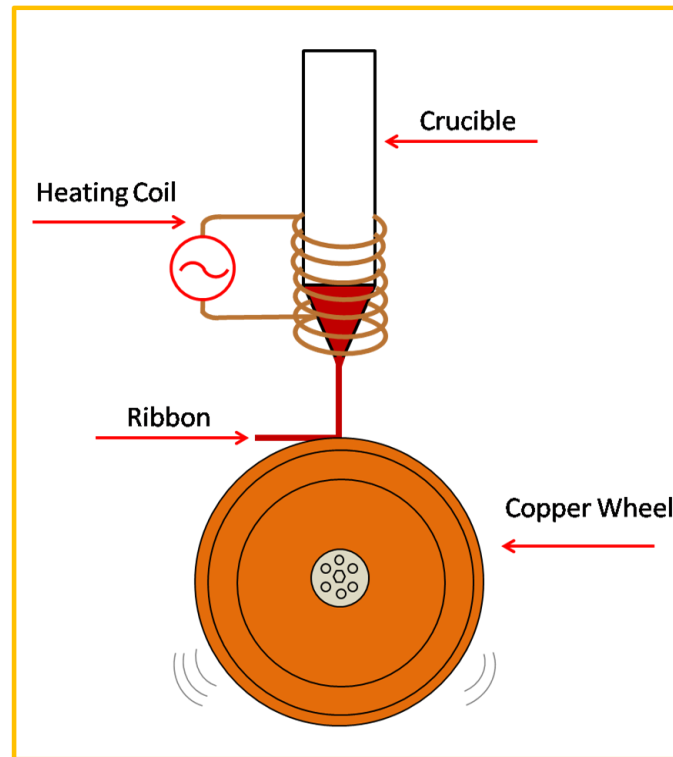
Figure 19.Schematic diagram of melt spinner.

3.3 Hysteresis Loop

The hysteresis loop is the fingerprint of a ferromagnetic material, the typical shape

can be seen in Figure 20, which results from a nonlinear response of ferromagnetic

materials to an applied external magnetic field. Any ferromagnetic material is composed

of small regions where all magnetic dipole moments align in the same direction, and

contiguous domains are separated by domain walls[59]. The hysteresis loop begins at a

starting point with zero applied field (H=0), at this state, all the domains are disoriented

such that vector sum of the magnetizations is zero. When an external magnetic field is

applied, the magnetization increase gradually and then rapidly, finally saturate at point a,

which is called saturation magnetization. In this point, the specimen becomes a single

domain that is aligned in the direction of applied field.When H is reversed and reduced to

zero, some magnetization remains, which is known as the remanence (B_r).This may be

explained by the resistance to movement of domain walls, corresponding to the increase

of H in the opposite direction[59]. In order to remove the remanence, a reversed H is

required. The field applied to reduce remanence to zero is called coercivity (H_c). Since all

the domains have different magnetization direction, there is no magnetic flux (B=0) at

point c.With increasing of field in the opposite direction, the same saturation happens as

it did before.The cycle is then reversed to get a full hysteresis loop.
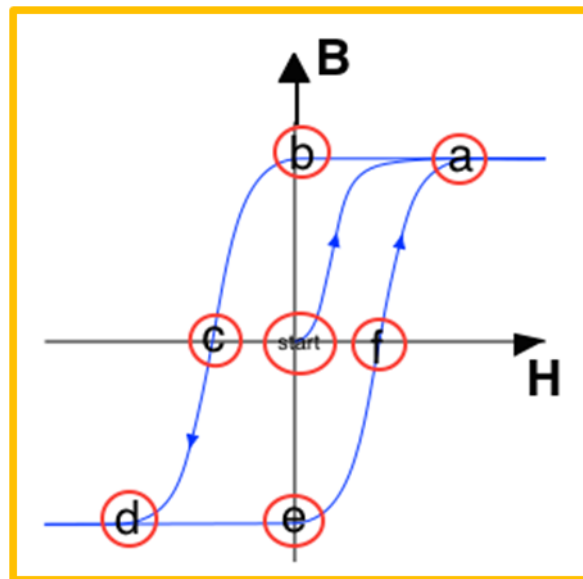
Figure 20. Schematic representation of a hysteresis loop for a ferromagnetic material portraying the saturation points (a and d), remanence points (b and e), and coercivity points (c and f)[60].
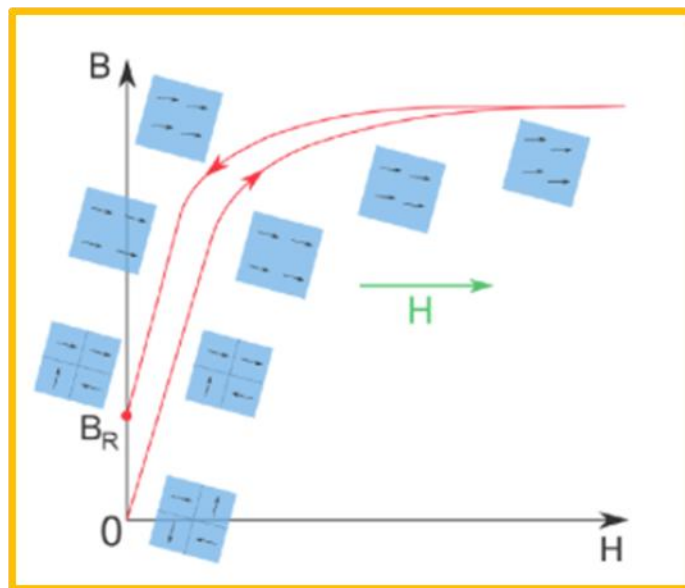
Figure 21. Schematic representation of the magnetic domains with increasing and decreasing magnetizing force[60]**.**

Figure 21 shows magnetic domains at different stages of magnetization. In the beginning, they are disoriented, and then gradually aligned with increasing magnetic field, finally misaligned again when moments cancel each other and yield zero net magnetic moment.

For hysteresis loop measurement, we used an alternating gradient magnetometer (AGM). The samples were mounted at the end of a holder by vacuum grease, and subjected to a fixed direct current (DC) field with an alternating field gradient.

3.4 X-ray Powder Diffraction

X-ray powder diffraction (XRD) is an analytical technique mainly used for identifying a material's crystal structure and phase fraction[61][62]. The basic process for

XRD can be described as three steps[56][57]. Firstly, X-rays are generated in cathode ray tube via heating a filament, then these X-rays are filtered by foils or crystal monochromators to produce monochromatic X-rays. Finally, these X-rays are collimated and directed to the sample. When the incident X-ray satisfies Bragg's Law, constructive interface leads to an observable intensity peak. A detector records this X-ray signal and counts the number of incoming X-rays at each angle. In this thesis, a PANalytical Empyrean diffractometer (Cu Kα radiation, λ=0.1541 nm, 45 kV and 40 mA) was used for XRD characterization.

Bragg's Law is classic principle used for XRD, which gives angle for coherent and incoherent scattering from a crystal lattice[63]. X-rays are scattered from lattice planes with interplanar spacing d, when the scattered waves interfere constructively, they remain in phase. It is because path length of every wave is equal to an integer multiple of the wavelength, which can be expressed by the equation 4. Here λ represents the wavelength of X-rays, n is a positive integer, d represents interplanar spacing, and θ represents diffraction angle.

$$n\lambda = 2d\sin\theta \tag{4}$$
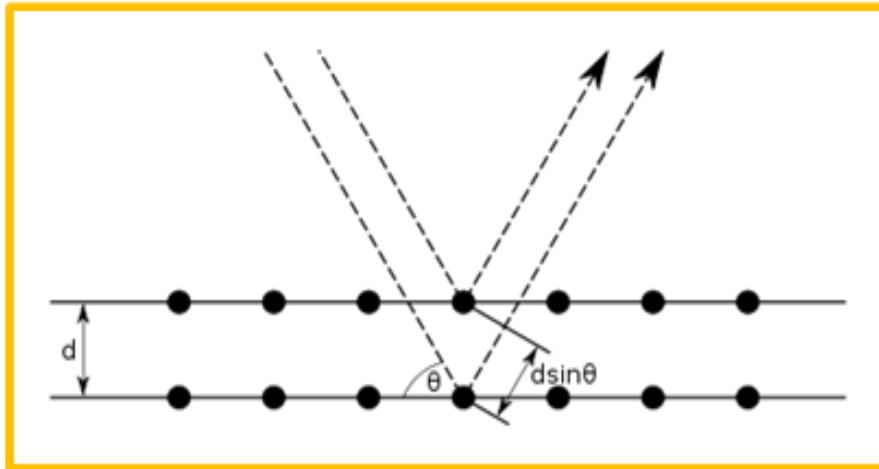
Figure 22.Bragg diffraction. Two beams with identical wavelength and phase approach a crystalline solid and are scattered off two different atoms within it. The lower beam traverses an extra length of 2dsinθ. Constructive interference occurs when this length is equal to an integer multiple of the wavelength of the radiation[63]**.**

3.5 Metallography

Metallography is a field of study on the physical structure and components of metals[64]. In our metallographic preparation process, Alnico ribbons were clamped by stainless steel cornings for a cross-section examination, and then were hot mounted by BUEHLER SIMPLIMET 1000 with hot compression thermosetting resin. After mounting, specimens were wet ground successively by SiC sandpapers with 400, 600, 800, 1200 grit to get a relatively smooth surface. Following with polishing by 1 micrometer Alpha Alumina powder to make sure there is no obvious scratches on the surface.

Light optical microscopy is a field of study using light microscope to view objects and areas of objects that cannot be resolved by naked eyes[65]. It magnifies view of

samples by passing visible light transmitted through or reflected from samples via a single or multiple lenses[66]. A Leica light optical microscope was used to examine the microstructures of Alnico ribbons.

3.6 Scanning Electron Microscopy

Scanning electron microscopy (SEM) is a technique that uses a focused electron beam to scan a sample. Through interaction of the electron beam and the sample, various signals are generated, such as secondary electrons, back-scattered electrons, and characteristic X-rays. Secondary electrons provide useful information about topography of the sample, while back-scattered electrons show atomic number contrast. The SEM is equipped with energy dispersive X-ray spectroscopy (EDS) to reveal the composition of the sample by using characteristic X-rays. In this thesis, all SEM images and EDS data were acquired by an FEI Helios NanoLab 660 operating at 10 kV and a working distance of 6.5 mm in imaging mode. Figure 23 shows the FEI Helios NanoLab 660.
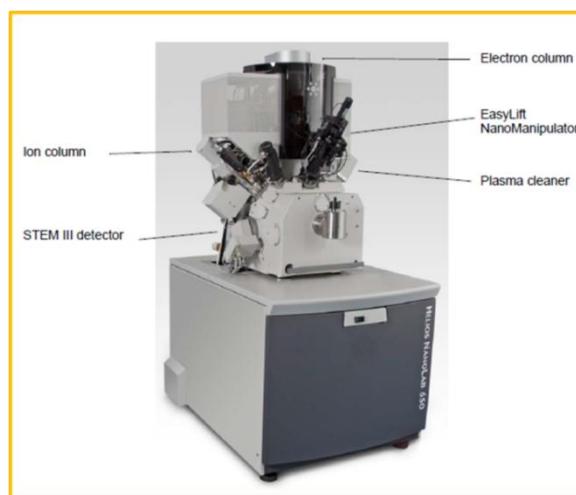
Figure 23. FEI Helios NanoLab 660

Chapter 4 Effect of Heat Treatment

4.1 Isothermal Heat Treatment

The coercivity of Alnico magnets arises from shape anisotropy, which despends on microstructure, such as the aspect ratio of α_1 phase, composition of α_2 phase, and interface microchemistry controlled by alloy composition and heat treatment process. Therefore, we report the effect of alloy composition and annealing on magnetic properties of Alnico in this chapter. The compositions similar to Alnico 8 and 9 were designed due to their potential for high coercivity and energy product. First of all, we described isothermal heat treatment process, which significantly controls microstructure. Then, we presented magnetic properties of the samples for different annealing processes.

The Alnico with compositions listed in table 3 were prepared for our study. Sample 1 and sample 2 are supposed to have high energy product and high coercivity[67], respectively. Sample 3 is typical Alnico 9. All of them were prepared by arc melting, and then melt spinning with the wheel speed of 40 mps. The width and thickness of the ribbons are about 2 mm and 30 μm, respectively. The melt-spun ribbons were wrapped with tantalum foil and then sealed in a quartz tube filled with argon. Some titanium granules were put into the quartz tube to prevent oxidation. The samples were isothermally heat treated at 780-830 °C for 10 minutes, followed with secondary annealing at 650 °C for 12 hours, and final annealing at 580 °C for 6 hours, as can be

seen in Figure 24.

Table 3.Compositions of Alnico Samples.

Sample	Al	Ni	Co	Cu	Ti	Fe	Nb
1(wt%)	8	14	42	3	6.5	26.5	0
2(wt%)	8.5	14	42	3	9.5	23	0
3(wt%)	7	15	35	4	5	33.5	0.5
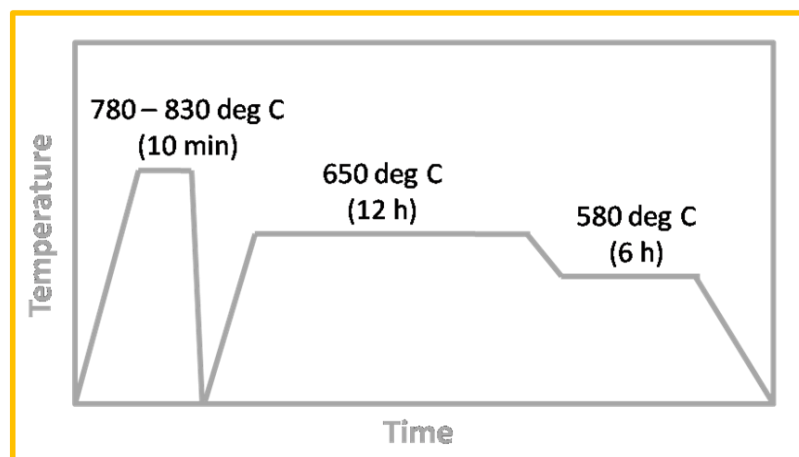
Figure 24. Schematic diagram for isothermal heat treatment process-temperature.
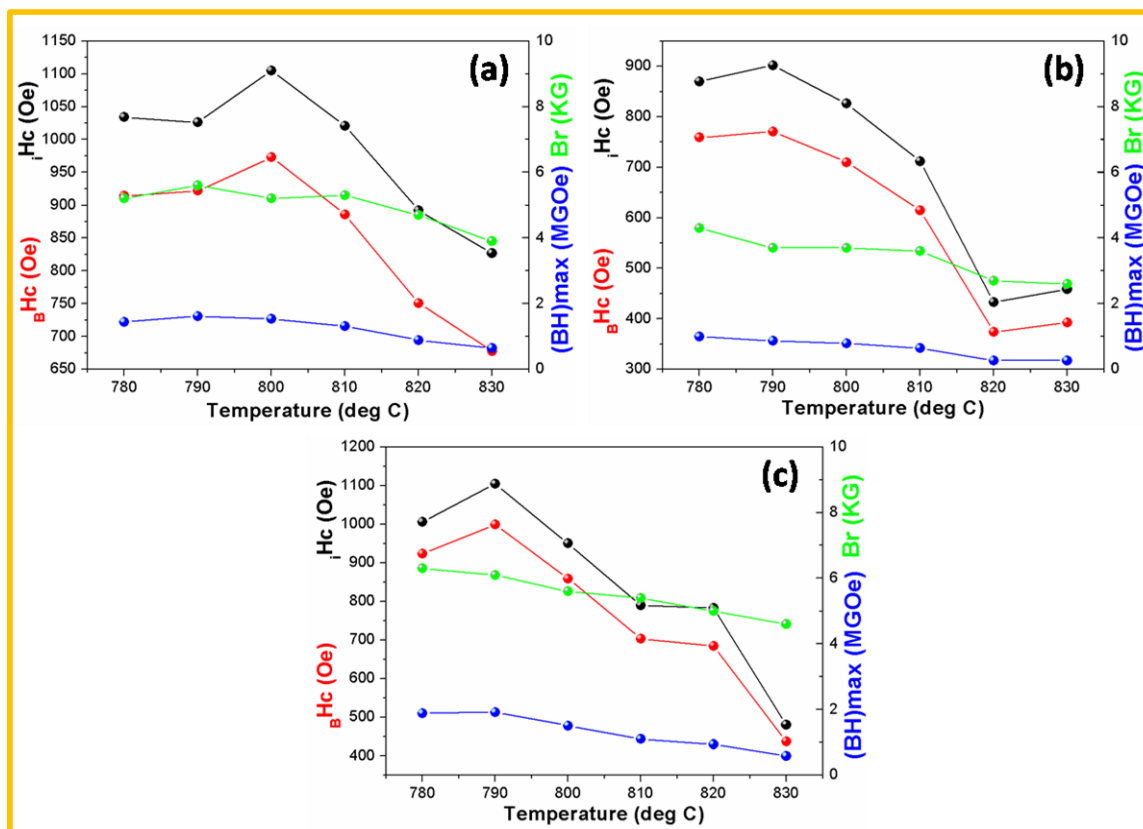
Figure 25. Effect of isothermal heat treatment temperature on magnetic properties of (a) sample 1, (b) sample 2 and (c) sample 3.

Figure 25 shows the effect of isothermal heat treatment (IHT) temperature on the magnetic properties of three Alnico samples. We can see that coercivity depends on IHT temperature, which first increases and then decreases with IHT temperature. Remanence and energy product gradually decrease with increasing temperature. The highest coercivity of the samples were obtained at 800 °C, 790 °C, 790 °C, respectively. It is because shape anisotropy is driven by microstructural evolution, which not only depends on spinodal decomposition but also particle coersening.

The composition fluctuation can be described by a sum of sinusoidal waves with various wavenumbers β[34], as be seen in equation 5. In the early stage of spinodal

decomposition, the sinosuidal wave with specific wavenumber will be selectively

amplified, dominating the decomposed structure[68][35]. For ferromagnetic materials,

the wavenumber is determined by free energy, elastic energy and magnetic energy

term[69][34].

$$\Delta c = c - c_0 = \sum_\beta A\cos\beta_r + B\sin\beta_r \tag{5}$$

where Δc is composition fluctuation, c is composition, c_0 is original composition, and

A and B are coefficients[34].

$$\beta_m^2 = -\left[\left(\frac{\partial^2 f_0}{\partial c^2}\right)_0 + 2\eta^2 Y_{100} + 4\pi\left(\frac{\partial M}{\partial c}\right)_0^2\right]/(4K) \tag{6}$$

here β_m is the maximum wavenumber, f is the free energy per unit volume of a

homogeneous alloys of composition c, K represents a gradient energy coefficient, η is the

fractional change in lattice parameter per unit composition change, and Y_{100} represents a

specialized elastic constant in the <100> direction [34].

$$K = N_v kT_c r_0^2/3 \tag{7}$$

where N_v is the number of atoms per unit volume, k is the Boltzmann constant, T_c is

spinodal decomposition temperature, and r_0 represents interatomic distance[34].

As we can see from equation 5 to 7, the microstructure is controlled by alloy

compositions and temperature, which explains various optimal isothermal heat treatment

temperature of the three samples.

An increase in characteristic length scale during microstructural evolution is called

coarsening[35]. Actual spinodal decomposition structures are irregular, which show

particle coarsening[70]. Equation 8 shows the evolution of the mean particle size[35].

$$< R(t) >^3 - < R(0) >^3 = \frac{8\widetilde{D}\gamma\Omega^2 C^{eq}(\infty)}{9kT} t = K_D t \tag{8}$$

where $R(t)$ is the mean particle size, $R(0)$ is original particle size, $\widetilde{D}$ is diffusivity, γ is interfacial energy, Ω is thermaldynamic potential, C^{eq} is the solubility of B atom in matrix phase for a system with a planar α/β interface, T is temperature, t is time, K_D is the rate constant for diffusion-limited coarsening.

The diffusivity increases with temperature exponentially[36]. When the isothermal temperature is high, the microstuctural evolution will develop dramatically. This could coarsen α_1 phase, and ruin shape anisotropy. Therefore, the balance between spinodal decomposition and particle coarsening is the key to optimal magnetic properties, which is determined by alloy compositions and heat treatment.

Since the optimal coercivity is achieved about 50-70°C below the spinodal decomposition temperature[44], we can conclude that Co could improve spinodal decomposition temperature while it is decreased by Ti.

We also investigated the effect of isothermal heat treatment time on magnetic properties of the Alnico samples. Schematic diagram of heat treatment process is shown in Figure 26.The optimal isothermal heat treatment time for sample 1, 2, and 3 is 20 minutes, equal to or less than 5 minutes, and 10 minutes, respectively. The coercivity trends for sample 1 and sample 3 are the same. Both of their optimal heat treatment time is between 5 and 10 minutes. However, the optimal annealing time for sample 2 is equal to or less than 5 minutes. Sample 1 has more Co content when compared with sample 3, which improves spinodal decomposition temperature. In addition the IHT temperaure

here (790 °C) is lower than the optimal one (800 °C), so more time is needed to complete

spinodal decomposition for obtaining optimal magnetic properties. Sample 2 has more Ti

content when compared with sample 1, which could reduce the spinodal decomposition

temperature. Thus, annealing time is shortened. By comparing sample 2 and sample 3, we

can see that IHT time is shortened for the sample with high Co and high Ti contents,

indicating Ti is more effective than Co to control IHT time.
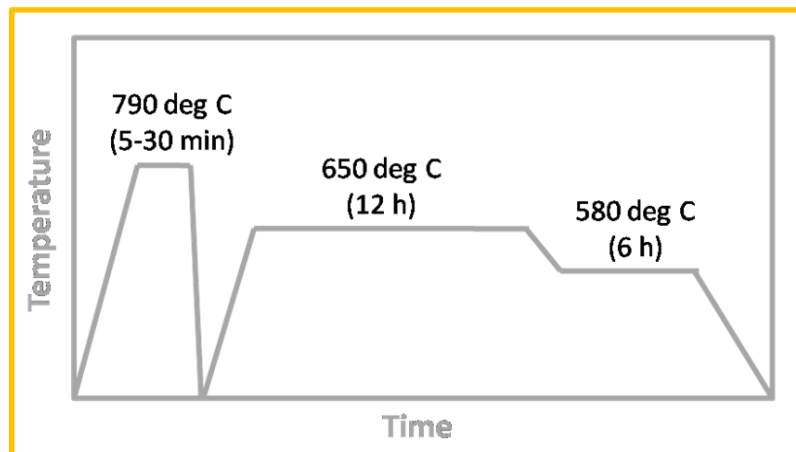
Figure 26. Schematic diagram for isothermal heat treatment process-time.
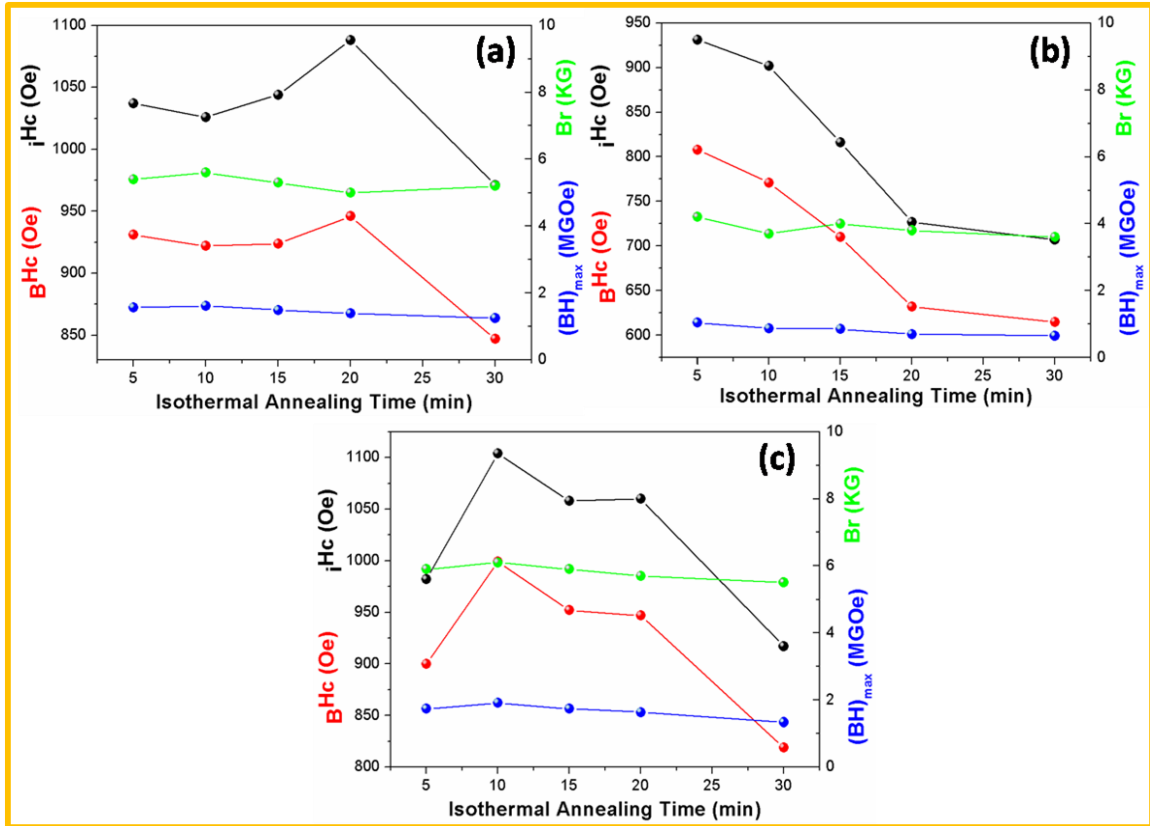
Figure 27. Effect of isothermal heat treatment time on magnetic properties of (a) sample 1, (b) sample 2 and (c) sample 3.

4.2 Secondary annealing

Secondary annealing (SA) or draw is a process used to sharpen α_1 phase. During secondary annealing, Fe-Co content in α_1 phase increase with decreasing temperature, while Fe-Co in α_2 phase decreases with decreasing temperature[41]. According to equation 2 and 3, this will increase the saturation magnetization difference between α_1 and α_2 phase, following with the improvement of coercivity. This can effectively improve magnetic properties, especially for coercivity, after isothermal heat treatment. Sample 1, sample 2 and sample 3 were isothermally heat treated at 790 °C for 10 minutes, and then

annealed at 630 °C to 670 °C for 12 hours, and finally annealed at 580 °C for 6 hours, as

can be seen in Figure 28. Figure 29 shows magnetic properties of the samples for

different SA temperature. As can be seen, there is no general trend, and the coercivity has

no discernable difference among them. It suggests diffusion and coarsening is limited at

these temperatures. It is also possible that the real trend is overshadowed by

microstructure variations among these ribbons, which will be discussed in the next

chapter.

The effect of SA time on magnetic properties was also studied. The samples were

isothermally heat treated at 790 °C for 10 minutes, and then annealed at 650 °C for 8

hours to 28 hours, and with final annealing at 580 °C for 6 hours. As can be seen in

Figure 31, magnetic properties of the samples are almost independent of SA time.
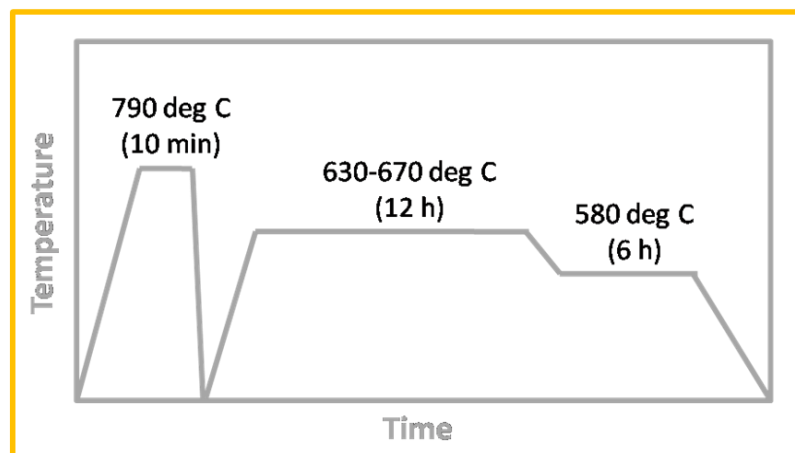
Figure 28. Schematic diagram for secondary annealing process-temperature.
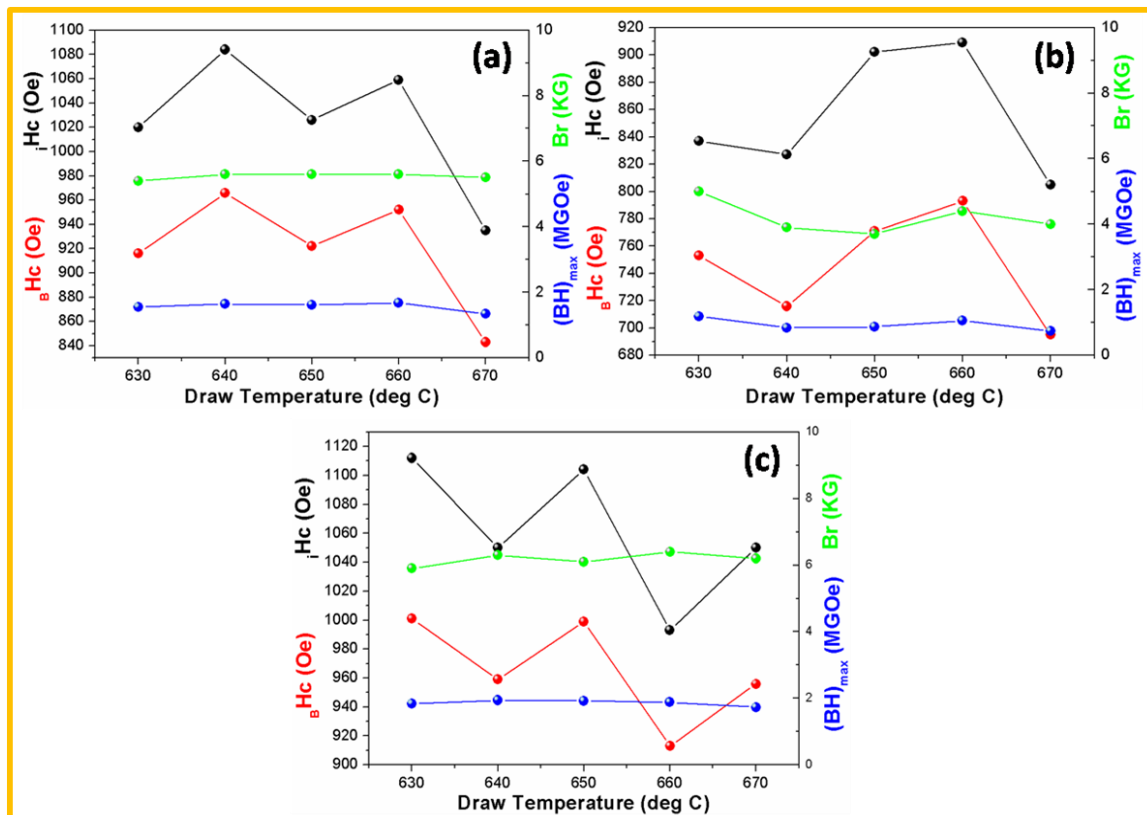
Figure 29. Effect of draw heat treatment temperature on magnetic properties of (a) sample 1, (b) sample 2 and (c) sample 3.
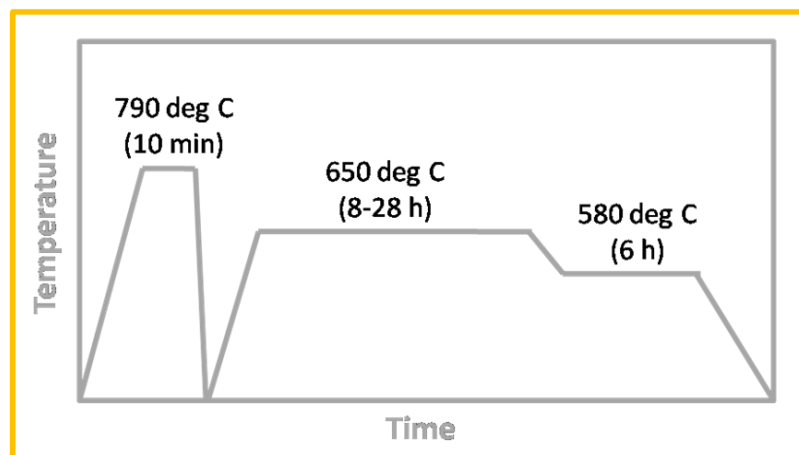
Figure 30. Schematic diagram for secondary annealing process-time.
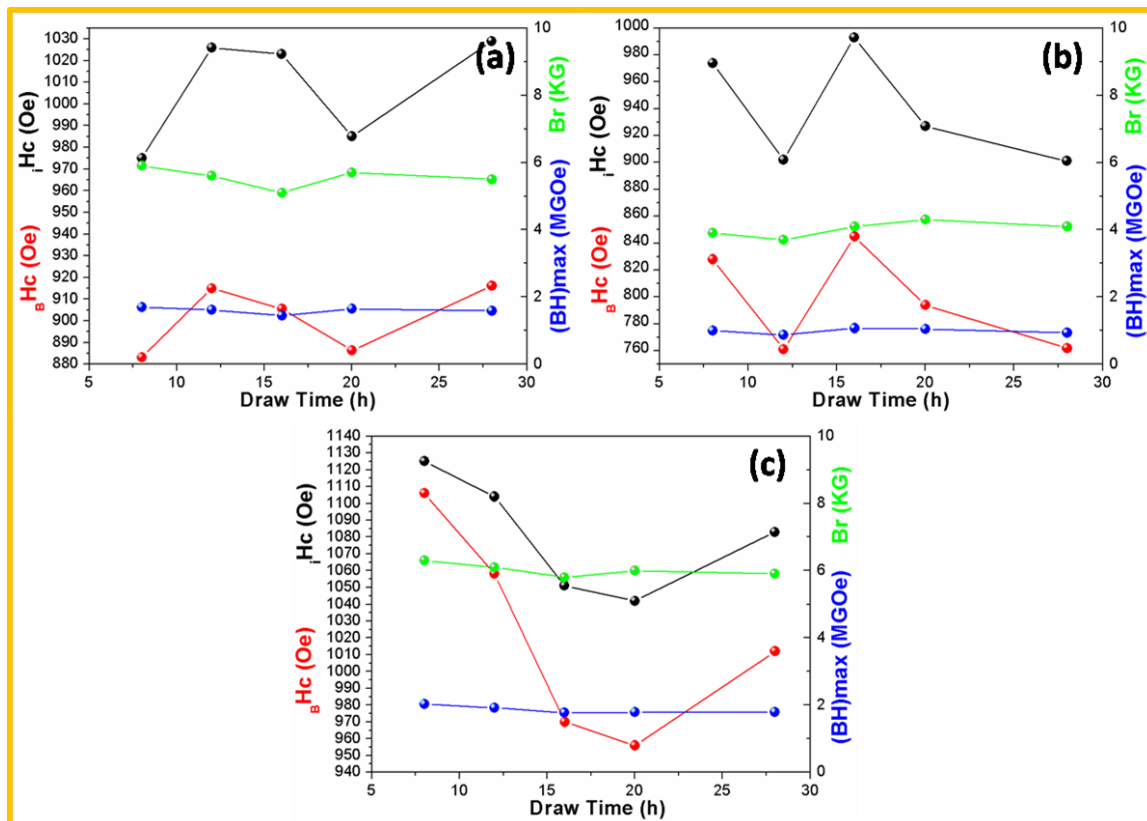
Figure 31.Effect of draw heat treatment time on magnetic properties of (a) sample 1, (b) sample 2 and (c) sample 3.

Chapter 5 Effect of Grain Microstructure

5.1 Wheel Speed

Magnetic properties of ferromagnetic alloys not only depend on intrinsic properties, but also microstructure, such as grain size, content of main phase, and phase distribution. For example, magnetic properties of neodymium magnets vary with the change of microstructure controlled by fabrication methods. In general, the coercivity of a neodymium magnet increases as the grain size decreases[71]. This is because that when the grain size is the same order of dimension as that of single domain particle, the domain wall is pinned at the grain boundaries, and a magnetic field higher than the pinning force is required to reverse the single-domain particle, following with higher coercivity[72]. This sheds light on our study of Alnico magnets. Although the origin and the improvement of magnetic properties of Alnico is different from neodymium magnets, it is possible that grain microstructure of Alnico influences its magnetic properties. In this chapter, we will study how grain microstructure controls magnetic properties of Alnico magnets by changing wheel speed.

Table 4.Composition of the sample.

Sample	Al	Ni	Co	Cu	Ti	Fe	Nb
(wt%)	7	15	35	4	5	31	3

We varied wheel speed, since it can change cooling rate, following with variation in microstructures. Ingots with compositions in Table 4 were prepared by arc melter, and then melt-spun with wheel speed at 10 mps, 15 mps, 20 mps, 30 mps and 40 mps, respectively. Interestingly, we found that ribbons spun at 10 mps, 15 mps and 20 mps are relatively brittle, while the ribbons spun at 40 mps are relatively ductile. The ribbons spun at 30 mps have both characteristics. These may influence their magnetic properties, which will be discussed later. As-spun ribbons were collected for microstructure characterization. The crystal structure and phase components of free side and wheel side of the as-spun ribbons were examined by XRD. For magnetic hysteresis loop measurement, the ribbons are sealed in argon, and isothermal heat treated at 790 °C for 10 minutes, and then rapidly quenched to room temperature, following with secondary annealing at 650 °C for 8 hours and third annealing at 580 °C for 18 hours.

Figure 32 shows variation of magnetic properties with increasing wheel speed. It is clear that the coercivity first increases and then decreases, which approaches to the maximum at 20 mps. The ribbons spun at 30 mps have relatively large standard deviation. Their remanence and energy product have no significant difference. There are two possible reasons for coercivity variation. Firstly, it is likely that coercivity of Alnico is grain microstructure dependent. Secondly, it could result from synergy of γ phase and grain microstructure. γ phase may form in our preparation process, especially for low wheel speed. Since we did not solutionize our samples, it is possible that α_γ phase exists in our annealed samples. The content of γ phase is inversely proportional to the wheel

speed. The increase of coercivity may arise from the reduction of γ phase content, while

the decrease of coercivity may be attributed to the formation of equiaxed crystals. The

competition of these two factors lead to the appearance of maximum coercivity at 20

mps.
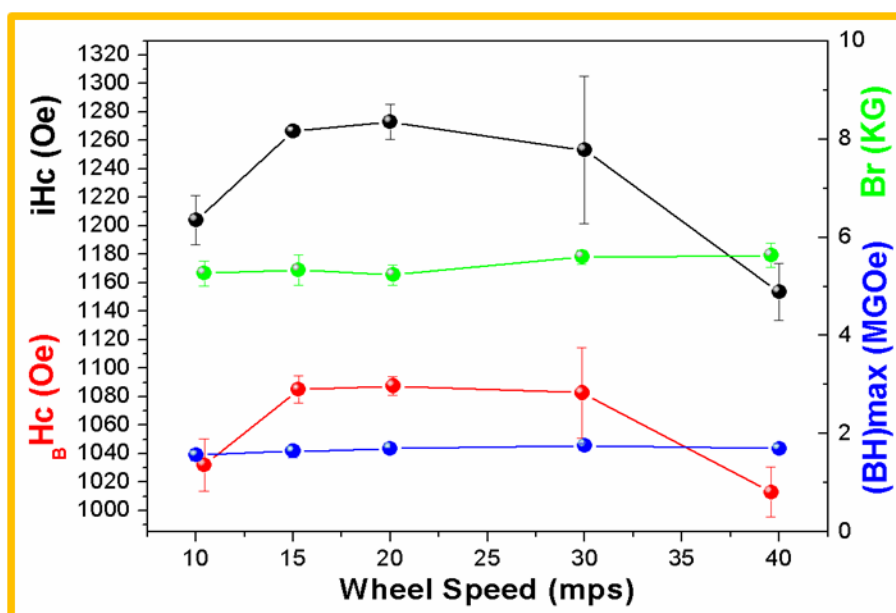
Figure 32. Effect of wheel speed on magnetic properties.

XRD patterns in Figure 33 shows diffraction peaks of ribbons spun at 10 mps, 20mps

and 40 mps, respectively. It seems there is no obvious difference among these samples,

expect for the free side of 10 mps, which shows strong diffraction at {200} peak,

indicating texture. Importantly, there is no γ phase diffraction peak at 10 mps, which

suggests there is no or minor γ phase formation in these samples.

Light optical microscope photomicrographs in Figure 34 show cross-sectional

microstructure of as-spun ribbons spun at 10 mps, 15 mps, 20 mps, 30 mps (ductile and

brittle) and 40 mps, respectively. We can see brittle ribbons spun at 30 mps have similar microstructure with ribbons spun at 15 mps, and microstructure of ductile ribbons spun at 30 mps is similar to the one spun at 40 mps, corresponding to their magnetic properties. Therefore, the large standard deviation of coercivity for the ribbons spun at 30 mps could result from the microstructure changes. However, the microstructures of the ribbons spun at 10 mps and 20 mps are comparable. For both of them, equiaxed grains composed of upper part, while columnar grains formed in the middle part of the ribbon. The difference is that columnar grains of the ribbons spun at 20 mps are aligned better than 10 mps, and the ribbons spun at 20 mps have more columnar grains. These could be beneficial for magnetic properties. It is also likely that there is a small amount of γ phase formation in the ribbons spun at 10 mps, due to its low cooling rate.
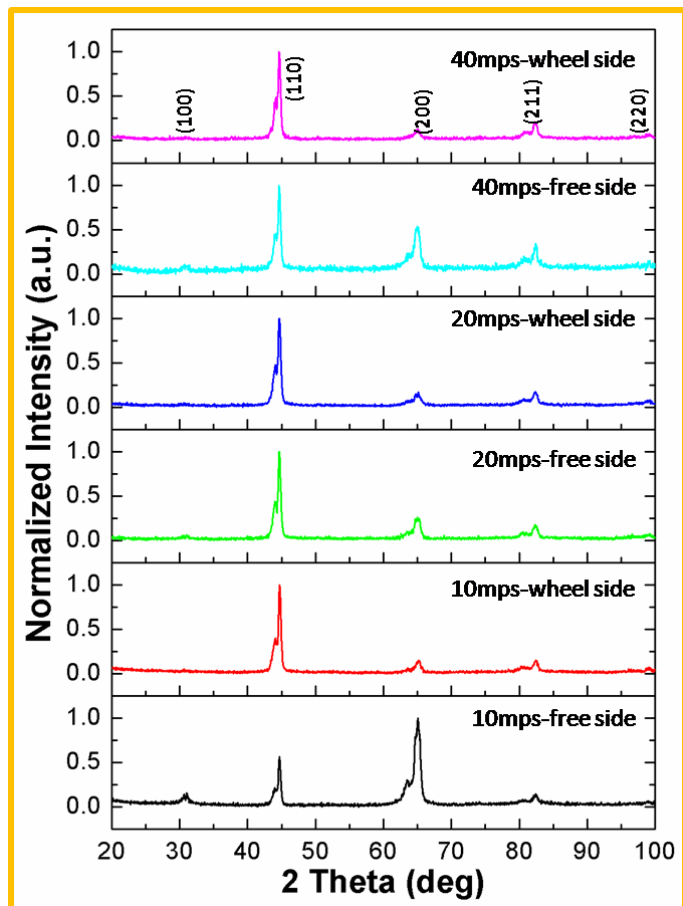
Figure 33. XRD pattern of the as-spun ribbons spun at 10 mps, 20 mps and 30 mps.
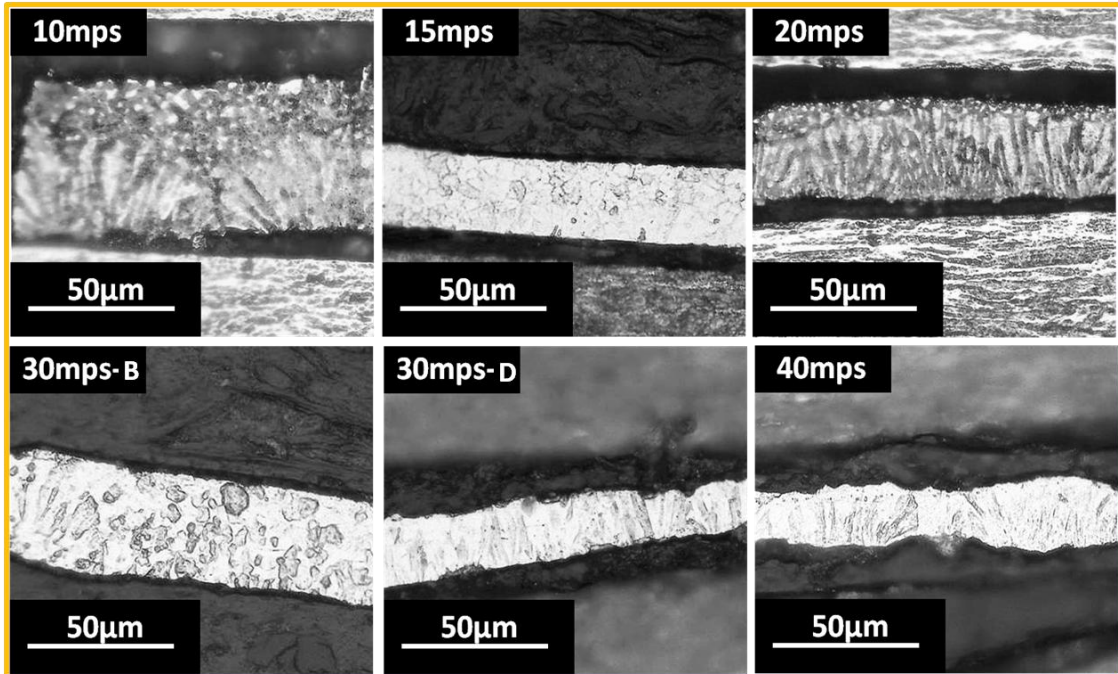
Figure 34. Cross-sectional light optical microscope photomicrographs of the as-spun ribbons spun at 10 mps, 15 mps, 20 mps, 30 mps (B: brittle and D: ductile) and 40 mps.

In conclusion, the coercivity of Alnico alloys is microstructure dependent. We can improve coercivity of Alnico alloys by tuning their microstructure. The optimal magnetic properties are obtained at 20mps.

5.2 Fabrication of Alnico with crystallographic texture

As we discussed in section 2.6.2, crystallographic texture in permanent magnet is beneficial for magnetic properties. We tried to further improve magnetic properties of Alnico by fabricating columnar grains. However, it is very difficult to get columnar grains in Ti-containing Alnico alloys unless texture enhancers are added. In order to get texture, two requirements must be satisfied, which are a steep temperature gradient and a

slow solidification rate[57]. Melt spinning is unfavorable for texture fabrication, due to its high cooling rate, which is on the order of 10^4-10^7 Kelvin per second[58]. Therefore, we set up a casting system to satisfy above requirements, as can be seen in Figure 35. The container of the mold was made by an alumina crucible. The bottom of the alumina crucible was machined to be open. The inner shell of the mold was made by the mixture of plaster, sand and water. The volume ratio for the mixture is plaster : sand : water = 21 : 21 : 15. The mixture was poured into the alumina crucible, and then a disposable centrifuge tube was used to make the center of the mold. The induction heat from the melt-spinner was employed to heat our sample. The sample was heated for over 5 minutes to make it reaches a temperature around or over 200 °C above its melting temperature. The mold was preheated to 1200 °C before pouring the molten Alnico. In this case, the heat was released into the chill copper. However, it should be stressed that the heat was also released into atmosphere by radiation and convection. The as-casted sample was ground and polished to remove the oxidation shell, and chill end of the sample was cut for characterization. Table 5 shows normal composition of the sample.

Table 5. Composition of the sample.

Element	Al	Ni	Co	Cu	Ti	Fe	Nb	S
(wt%)	7	15	35	4	5	33.3	0.5	0.2

Figure 36 shows XRD pattern of the as-casted sample. It is clear that {200} diffraction peak is dominant peak, indicating crystallographic texture was formed in our sample. For magnetic properties measurement, the sample was isothermally heat treated at 790 °C for 10 minutes, and then was rapidly quenched to room temperature, following with tempering at 650 °C for 8 hours and 580 °C for 18 hours, respectively. Both hysteresis loops with magnetic field parallel and perpendicular to the sample surface were measured, as can be seen in Figure 37. However, it seems the magnetic properties of textured Alnico are not as good as melt-spun ones. There is slightly difference between the parallel hysteresis loop and perpendicular one, which means the sample is slightly anisotropic or isotropic. It is likely that the simple casting system may not generate strong texture in Ti-containing Alnico because of heat transfer to atmosphere. Furthermore, a continuous casting is not practical in small scale experiment. Therefore, a steep temperature gradient is not available during the process. In addition, slow solidification rate resulted in the formation of γ phase in our sample, and the magnetic properties were further deteriorated by S addition.

In summary, we successfully fabricated textured Ti contained Alnico alloy by setting up a casting system. However, the comparison between the parallel and perpendicular hysteresis loop shows its slightly anisotropic or isotropic character.This is because a stable temperature gradient is not available in our simple casting system, following with tilt of columnar crystals. Moreover, its magnetic properties have no further improvement when compared with melt-spun ones, which results from the deleterious effect of γ phase

and S addition.
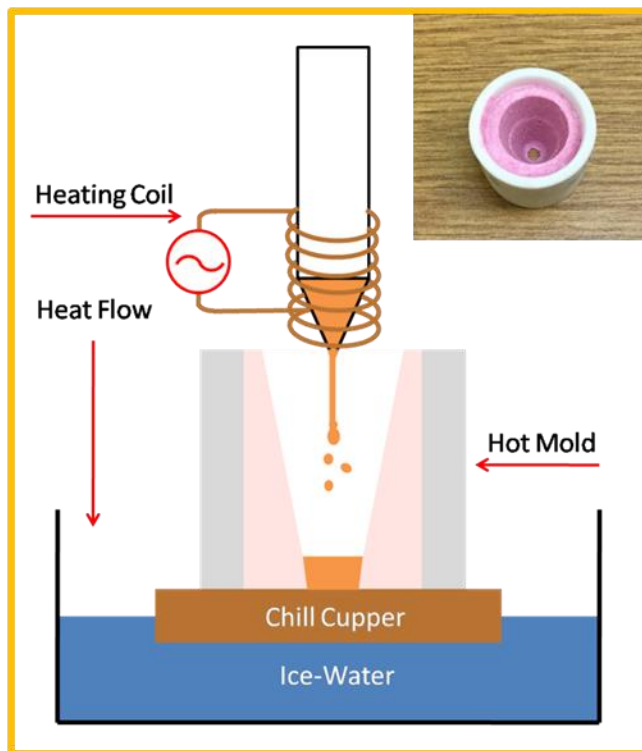
Figure 35.Schematic diagram of casting system.
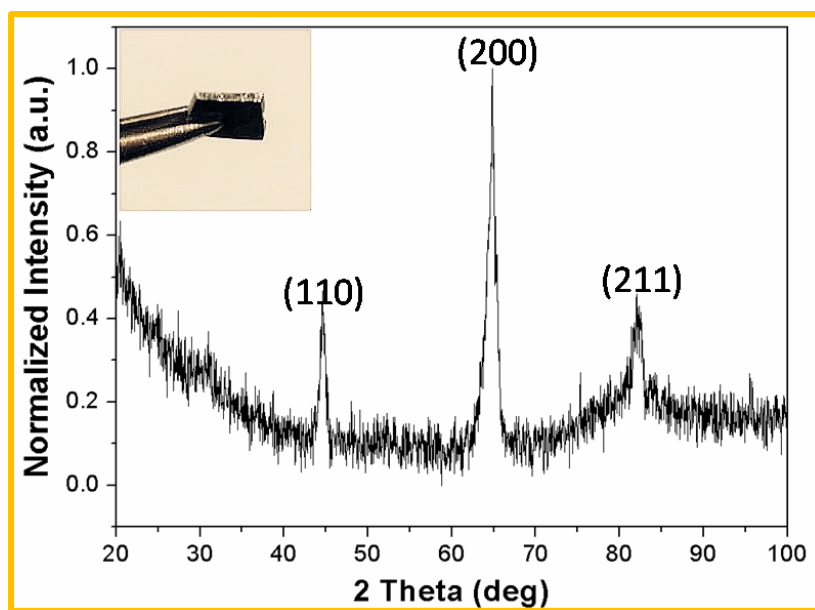
Figure 36.XRD pattern of textured Alnico 9.
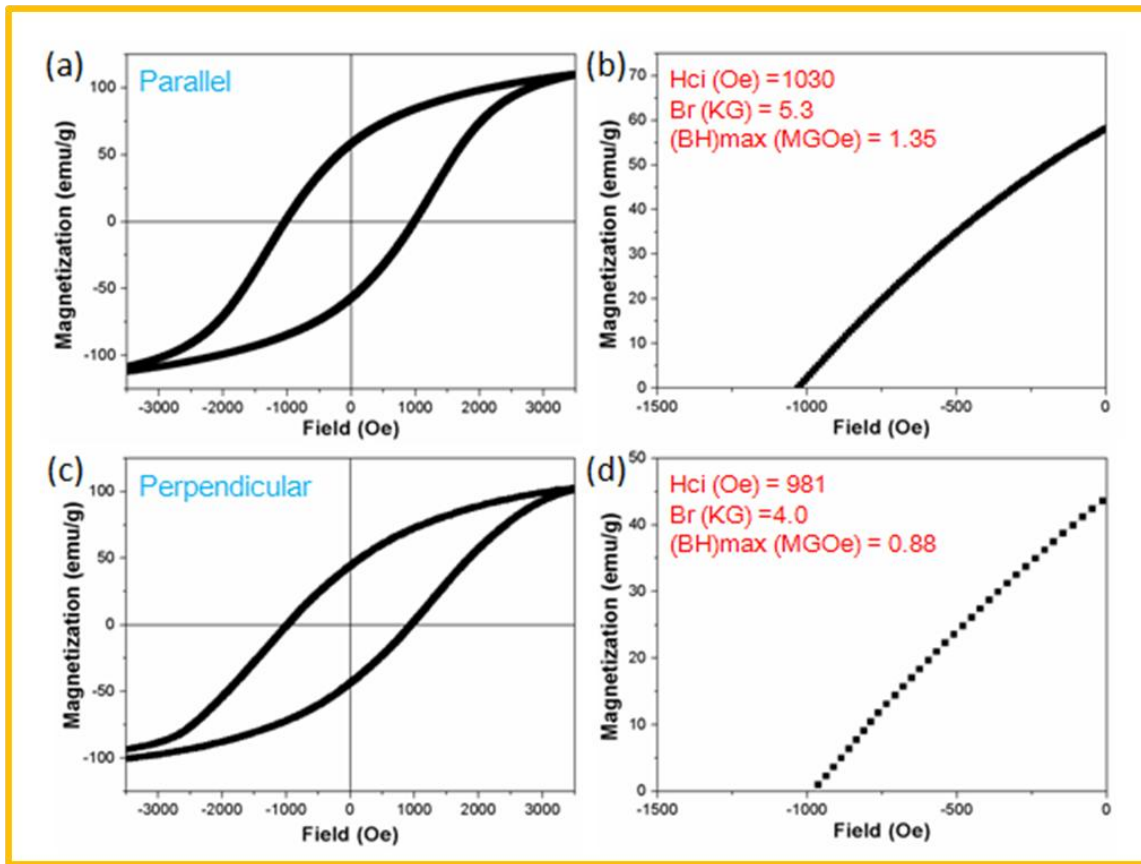
Figure 37. Hysteresis loop of textured Alnico 9.

Chapter 6 Avoidance of gamma phase by alloying addition

γ phase is a FCC phase, which is detrimental to magnetic properties of Alnico. As seen in Figure 38, γ phase is stable at temperature range from 860 °C to 1200 °C. In order to avoid γ phase, researchers tried to quench Alnico alloys from their homogenized state, which effectively avoids γ phase transformation. However, the solutionization requires high temperature furnace. This is not cost-effective for industry production. Furthermore, as we discussed in section 2.5, it is hard to solutionize high Co-containing Alnico alloys without destroying grain microstructures, since the temperature range of γ phase almost coincides with the solidus of Alnico. Here, we were interested in alloying addition, which could also avoid γ phase formation in Alnico without high temperature solutionization.
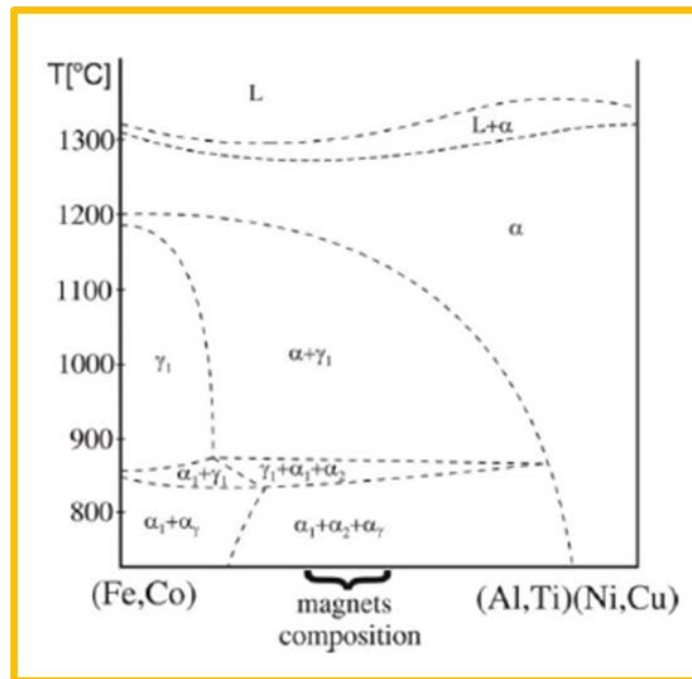
Figure 38. Phase diagram of Alnico alloys[41].

6.1 Effect of Sn addition

Compositions of the Alnico alloys are shown in Table 6, x is in the range of 0 to 3 wt%. The effect of Sn addition on magnetic properties of Alnico were characterized by hysteresis loop after the heat treatment 1: the ribbons were isothermally heated at 790 °C at 10 minutes and then quenched to room temperature, following with secondary annealing at 650°C for 8 hours and third annealing at 580 °C for 18 hours. To investigate the effect of Sn on γ phase avoidance, we did γ heat treatment (the heat treatment 2): ribbons were heated at 1100 °C for 1 h to generate more γ phase, and then quenched to room temperature, following with heat treatment 1. The schematic diagrams for the heat treatment 1 and 2 are shown in Figure 39.
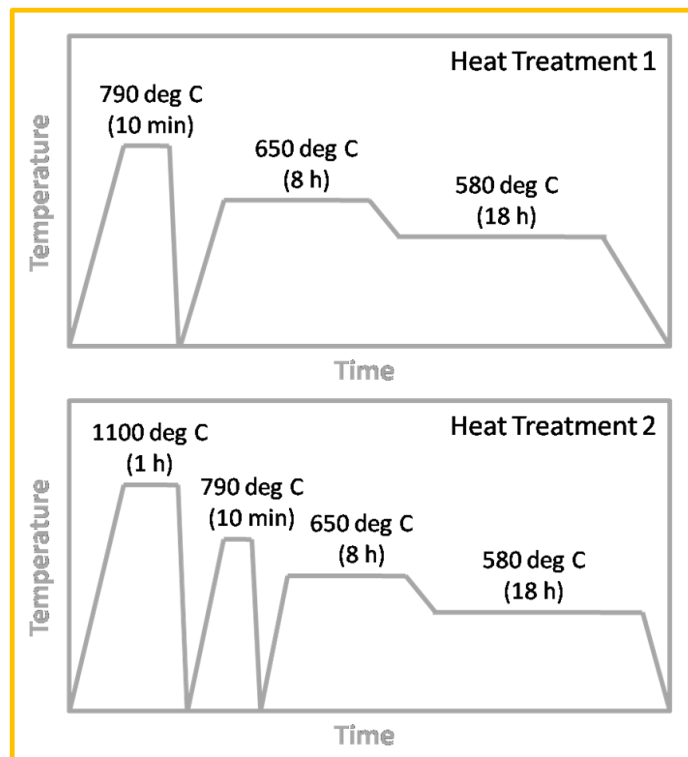
Figure 39.Schematic diagram of heat treatment 1 and 2.

Table 6.Compositions of the samples.

Element	Al	Ni	Co	Cu	Ti	Nb	Sn	Fe
(wt%)	7	15	35	4	5	3	x	balance
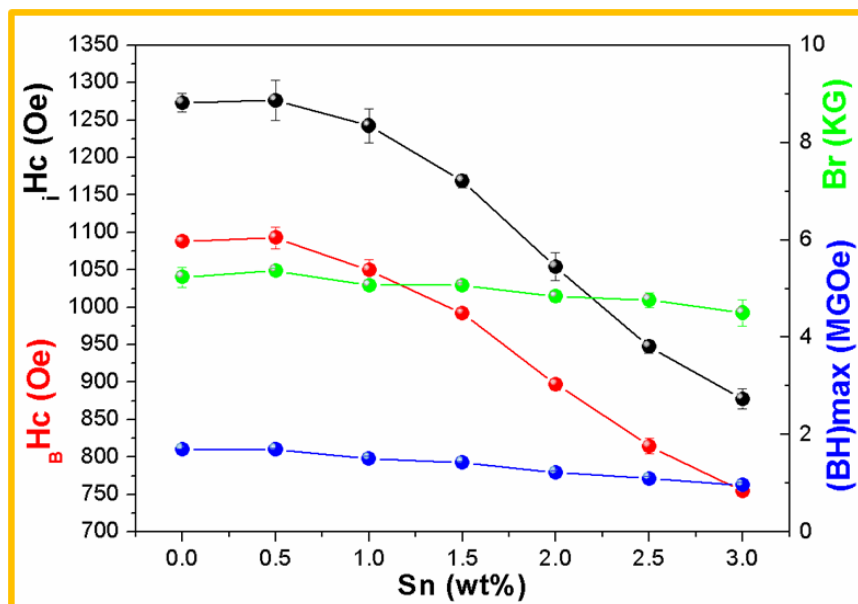
Figure 40.Effect of Sn on magnetic properties of the Alnico alloys.

Figure 40 shows variation of magnetic properties of the Alnico alloys with increasing

Sn addition after heat treatment 1. It is clear that magnetic properties have no obvious

change when x<0.5 wt%, while magnetic properties monotonically decrease with

increasing Sn when x>0.5 wt%. It is possible that Sn enters α_1 phase, which reduces the

difference in saturation magnetization between α_1 and α_2 phase, resulting in coercivity

deterioration.

Figure 41 shows magnetic properties of the Alnico samples versus increasing Sn

content after heat treatment 2. As we can see, coercivity increases monotonically when x

range from 0 to 1 wt%. However, it drops when x>1. Remanence and energy product are

not sensitive to Sn addition. This suggests that 0 to 1 wt% addition of Sn is effective to

remove γ phase inAlnico alloys. It is likely that Sn could avoid the formation of γ phase

or narrow the temperature range where γ phase is stable, following with better magnetic

properties. When x>1, there might be some phases formed which have deleterious effect

on magnetic properties. It is also possible that Sn enters α_1 phase, lowering shape

anisotropy, which overshadows its effect of γ phase avoidance. In order to investigate the

reasons, we performed XRD, SEM and EDS.

XRD patterns in Figure 42 show that there is a diffraction peak from γ phase for γ

phase heat treated Alnico without Sn addition. In contrast, there is no diffraction peak

corresponding to γ phase for 1 wt% Sn-containingAlnico. The XRD pattern of Alnico

with 3 wt% Sn addition is different from above, suggesting there was an impurity phase

formed. We can also see that diffraction peak corresponding to α_2 shifts towards lower

2θ with increasing Sn, which suggests Sn dissolves into $\alpha_2$phase.

Figure 43 shows cross-sectional SEM pictures of Sn-containing Alnico ribbons. It is

clear that there was a impurity phase formed with increasing Sn content. Figure 44 shows

EDS spectra of the area with the impurity phase and the area without the impurity phase.

It seems that there is no obvious difference between the compositions of the area with

impurity phase and the area without impurity phase. It is very likely that the impurity

phase is too small, so EDS does not only collect characteristic X-rays from the impurity

phase, but also surrounding areas without the impurity phase.
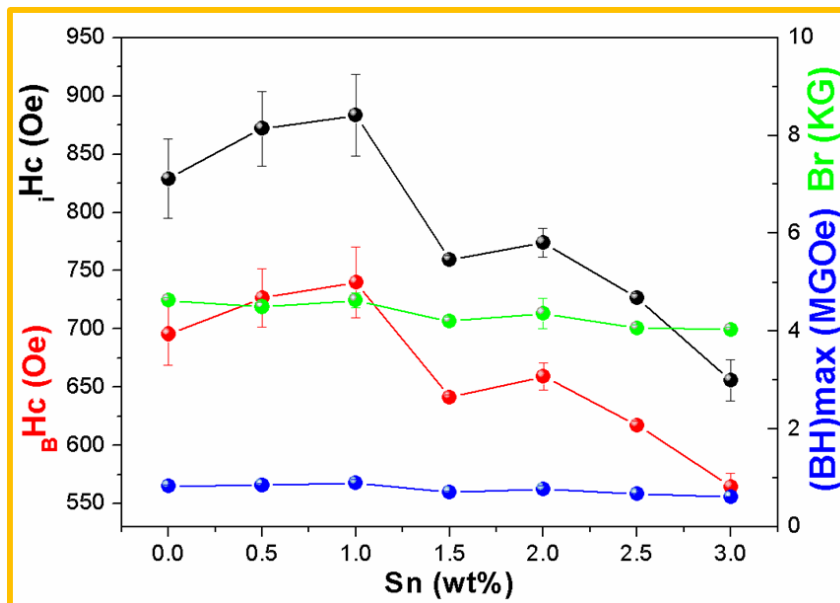
Figure 41. Effect of Sn on magnetic properties of γ heat treated Alnico alloys.
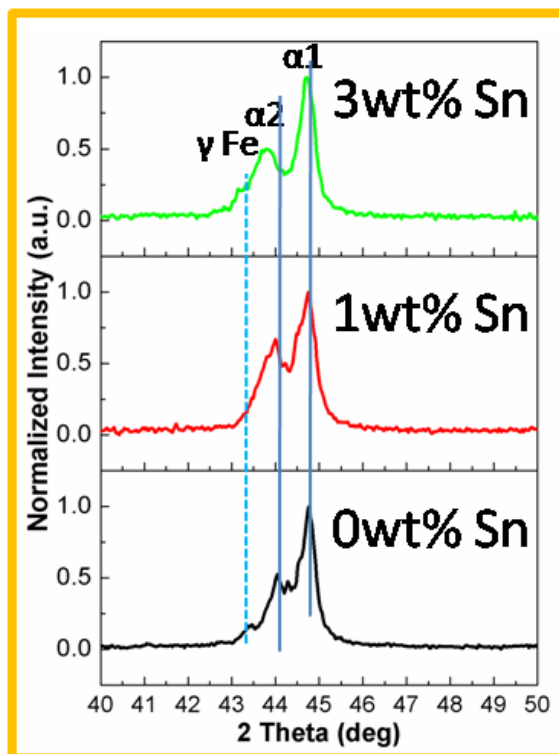
Figure 42. XRD pattern of γ heat treated Alnico alloys.
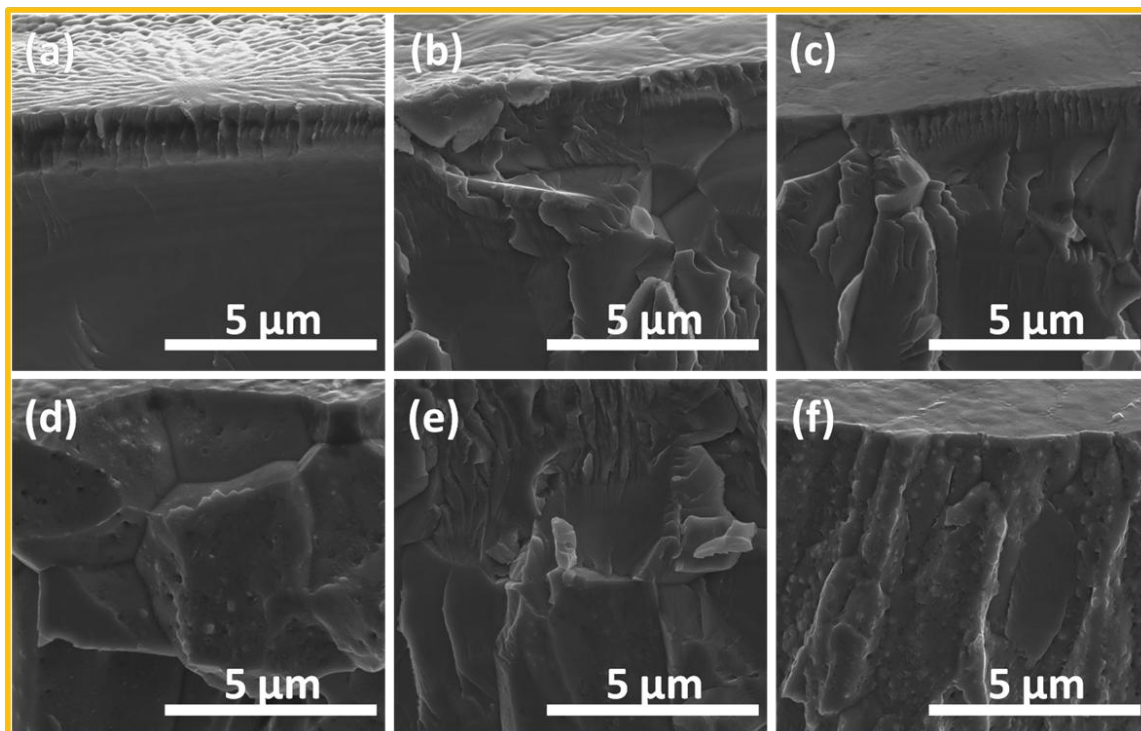
Figure 43.Cross-sectional SEM images of Sn-containing Alnico ribbons.
Alnico ribbons with (a) 0.5 wt%, (b) 1wt%, (c) 1.5 wt%, (d) 2 wt%, (e) 2.5 wt% and
(f) 3 wt% Sn.
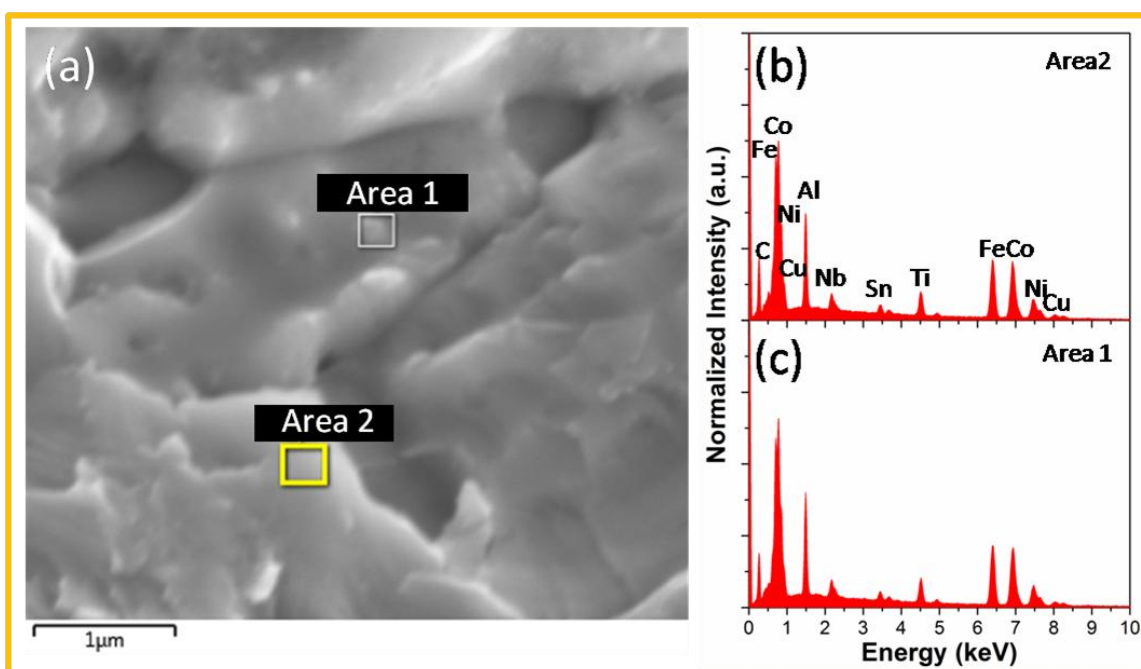
Figure 44. Cross –sectional SEM image and EDS spectra of Alnico ribbons with 3 wt%
Sn. (a) SEM image, (b) EDS spectra of the area without impurity phase and (c) with

impurity phase.

Table 7. Compositions of the area with impurity phase and the area without impurity phase.

Area	Al	Ni	Co	Cu	Ti	Nb	Fe	C	Sn
1(wt%)	6.4	12.7	29.4	6.1	3.9	2.6	23.2	13.4	2.4
2(wt%)	6.1	12.5	28.6	5.9	3.9	2.6	22.5	15.5	2.4

6.2 Effect of Ge addition

We also found Ge has a similar effect on restraining the generation of γ phase. The composition of our samples is shown in Table 8. The specimens were heat treated in two different ways, as in section 6.2. For heat treatment 1, the samples were heat treated at 810 °C for 10 minutes, followed by secondary annealing at 650 °C for 12 hours, and final annealing at 580 °C for 6 hours. For heat treatment 2, the samples were heat treated at 1100 °C for 1 hour, and then quenched to room temperature, followed by heat treatment 1. The schematic diagram for the heat treatments is shown in Figure 45.

Table 8.Compositions of the samples.

Sample	Al	Ni	Co	Cu	Ti	Ge	Fe
1(wt%)	7	14	40	3.5	4	0	balance
2(wt%)	7	14	40	3.5	4	1	balance
3(wt%)	7	14	40	3.5	4	5	balance
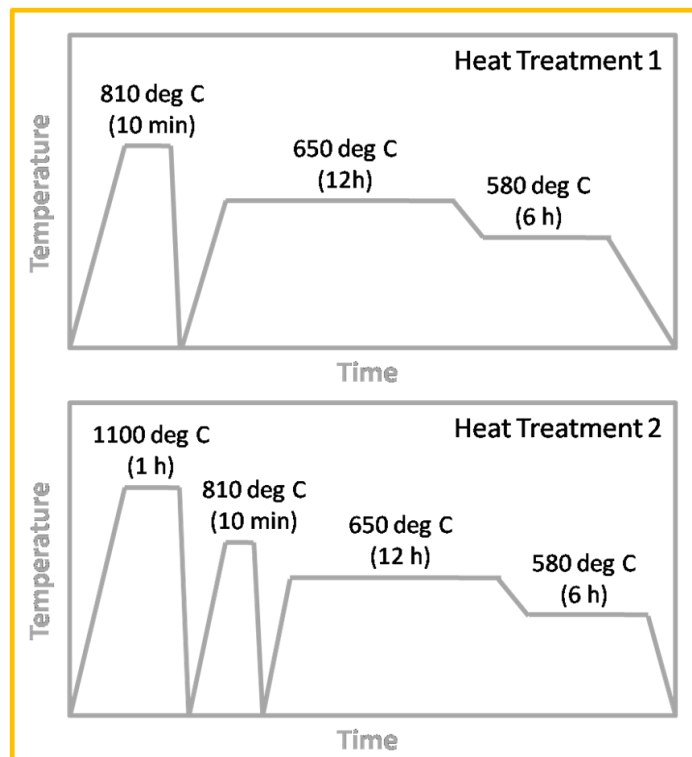
Figure 45. The schematic diagrams of heat treatment 1 and 2.
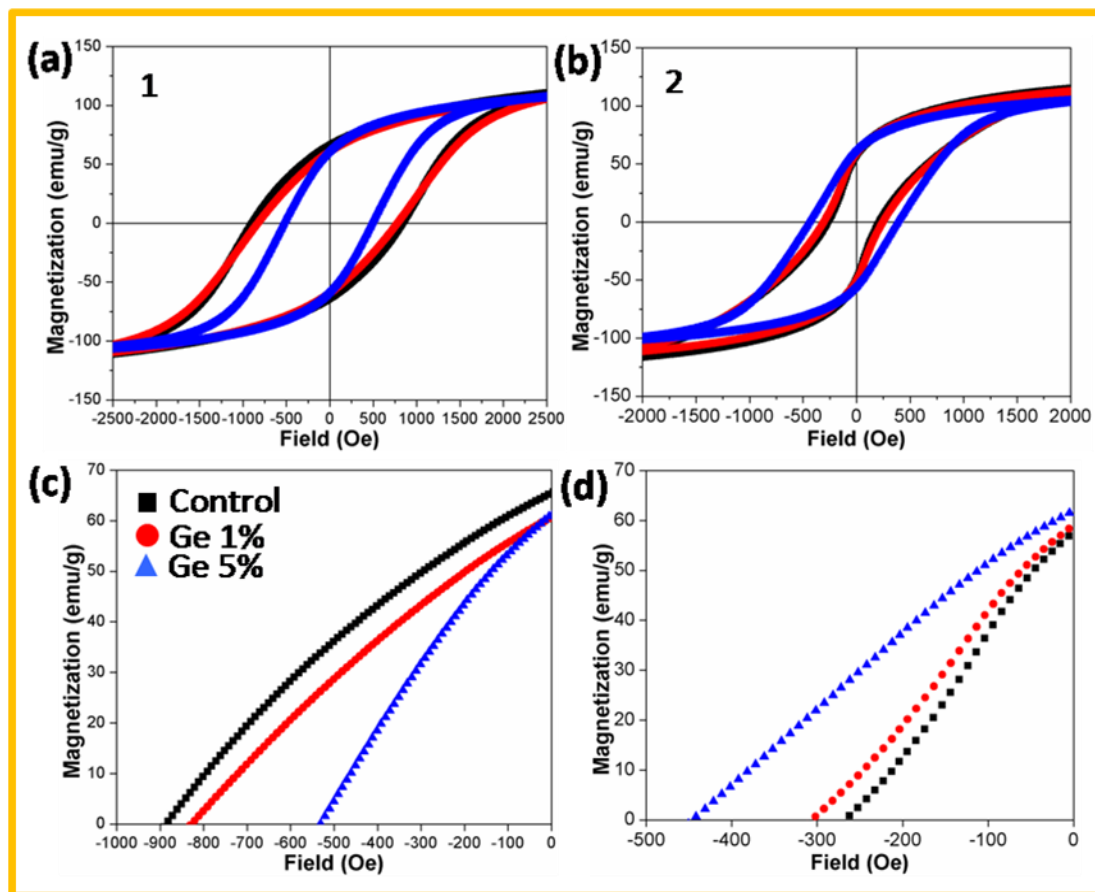
Figure 46. Effect of Ge on magnetic properties of Alnico alloys. (a) full and (c) second quadrant hysteresis loops of the samples after heat treatment 1, (b) full and (d) second quadrant hysteresis loops of the samples after heat treatment 2. (black square represents control, red dot respresents1 wt% Ge-containing sample, blue triangle represents the 5 wt% Ge-containing sample)

As can be seen in Figure 46 (a)(c), 1 wt% Ge addition slightly reduces coercivity of Alnico by about 100 Oe. However, 5 wt% Ge addition decreases the coercivity about 43%. As for heat treatment 2, we generate more γ phase in the samples. Therefore, we can determine how effective the Ge is by comparing them. Figure 46 (b) (d) show the sample with 5 wt% Ge has the best coercivity, followed by the 1 wt% Ge-containing sample. This suggests that Ge is effective in suppressing the formation of γ phase in Alnico magnets.

In addition, we compared the XRD patterns of these samples, as can be seen in Figure 47. The relative intensity of diffraction peak from γ phase decreases with the increase in Ge content, indicating that γ phase gradually decreases with Ge addition. It implies that Ge addition suppressed the formation of γ phase in Alnico magnets.
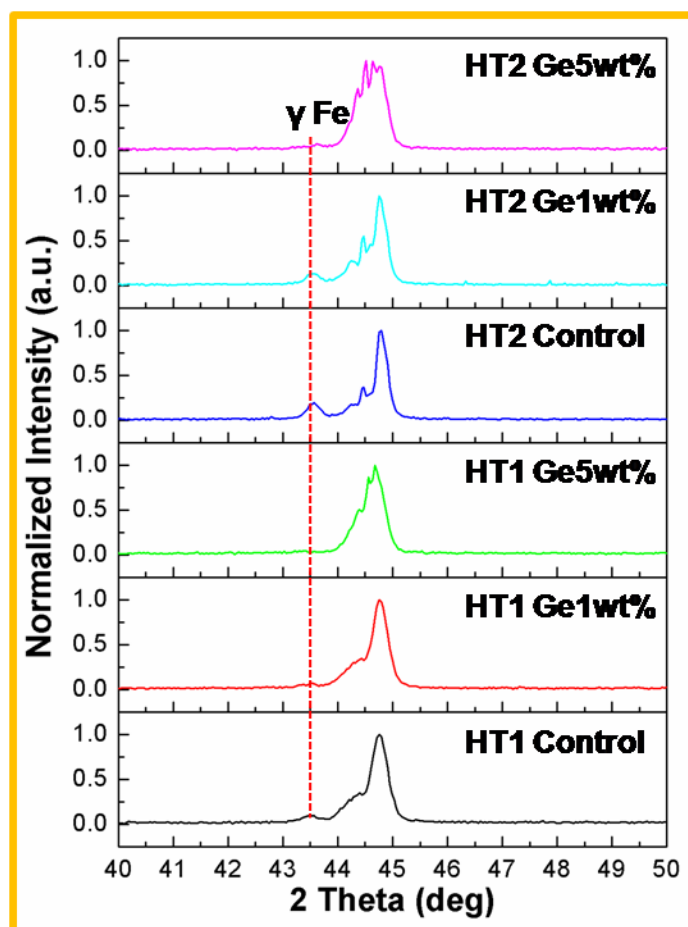
Figure 47. XRD pattern of the Alnico samples after heat treatment 1 and 2. (HT1 indicates heat treatment 1, HT2 indicates heat treatment 2)

Chapter 7 Effect of Field Annealing

α_1 phase spontaneously aligns in crystallographic <100> direction, since it's an

energy-favorable direction[34]. However, <100> is the family of [100], [010], [001]

directions, which means Fe-Co rich phase will align in three directions without applied

magnetic field. In order to obtain anisotropy, a magnetic field is applied so that α_1 grows

in only one of the three <100>. This will not only improve coercivity, but also remanence

and energy product. Therefore, we investigated the effect of magnetic field on magnetic

properties of melt-spun Alnico alloys.
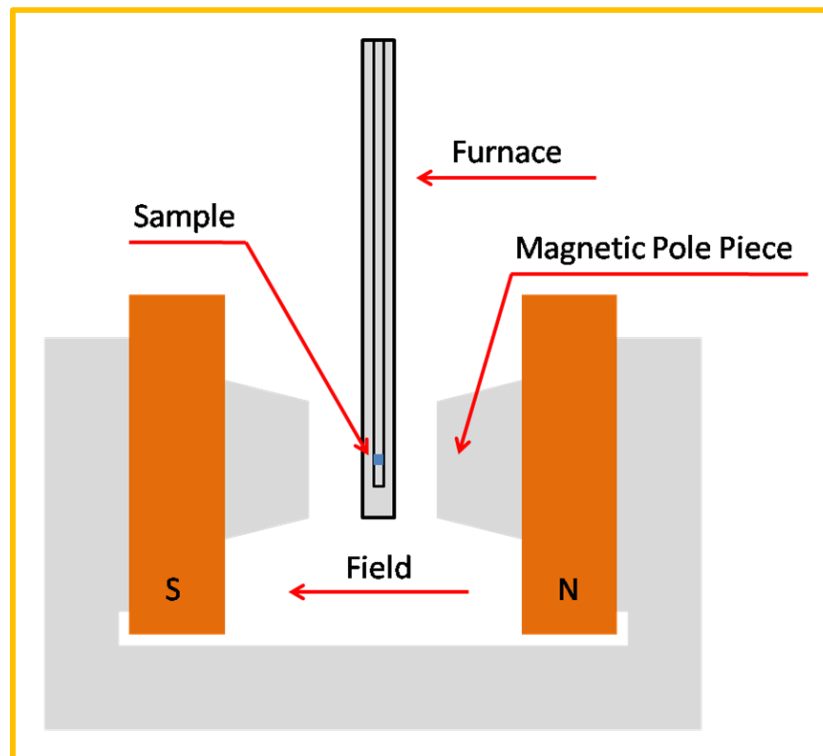
Figure 48. Field annealing set up.

Table 9. Compositions of the samples.

Sample	Al	Ni	Co	Cu	Ti	Nb	Fe
1(wt%)	8	14	38	3	8	0	balance
2(wt%)	8	14	38	3	8	3	balance
3(wt%)	7.3	13	38	3	6.4	3	balance
4(wt%)	7	15	35	4	5	3	balance

Figure 48 shows the set up for field annealing. The field is applied by the magnetic pole piece of a vibrating sample magnetometer (VSM). The samples with compositions in Table 9 were field annealed from 770 °C to 810 °C for 10 minutes. 9000 Gauss magnetic field was applied for the whole process. Samples were furnace cooled and their magnetic properties were measured after field annealing.

Figure 49 shows the effect of magnetic field on coercivity of the Alnico samples. It is clear that magnetic field decreases optimal IHT temperature. The presence of a magnetic field during spinodal decomposition may change the magnetic energy term. This could control microstructural evolution, as can be seen in equation 6. Therefore, the optimal temperature is lowered. This can also be used to explain that the magnetic field improves shape anisotropy at relatively low IHT temperature, but destroys it at relatively high IHT temperature. As we can see, the effectiveness of magnetic field also depends on composition of the samples. For sample 1 and sample 2, it seems that the magnetic field

cannot improve their coercivity. In contrast, the presence of a magnetic field improves

coercivity of sample 3 and 4 when IHT temperature is below 790 °C.This may result

from composition variation of α_1 phases in these samples, followed by different

ferromagnetic properties. The effects of magnetic field on remanence and energy product

are shown in Figure 50 and Figure 51, respectively. As can be seen, both remanence and

energy product are improved by the presence of magnetic field.
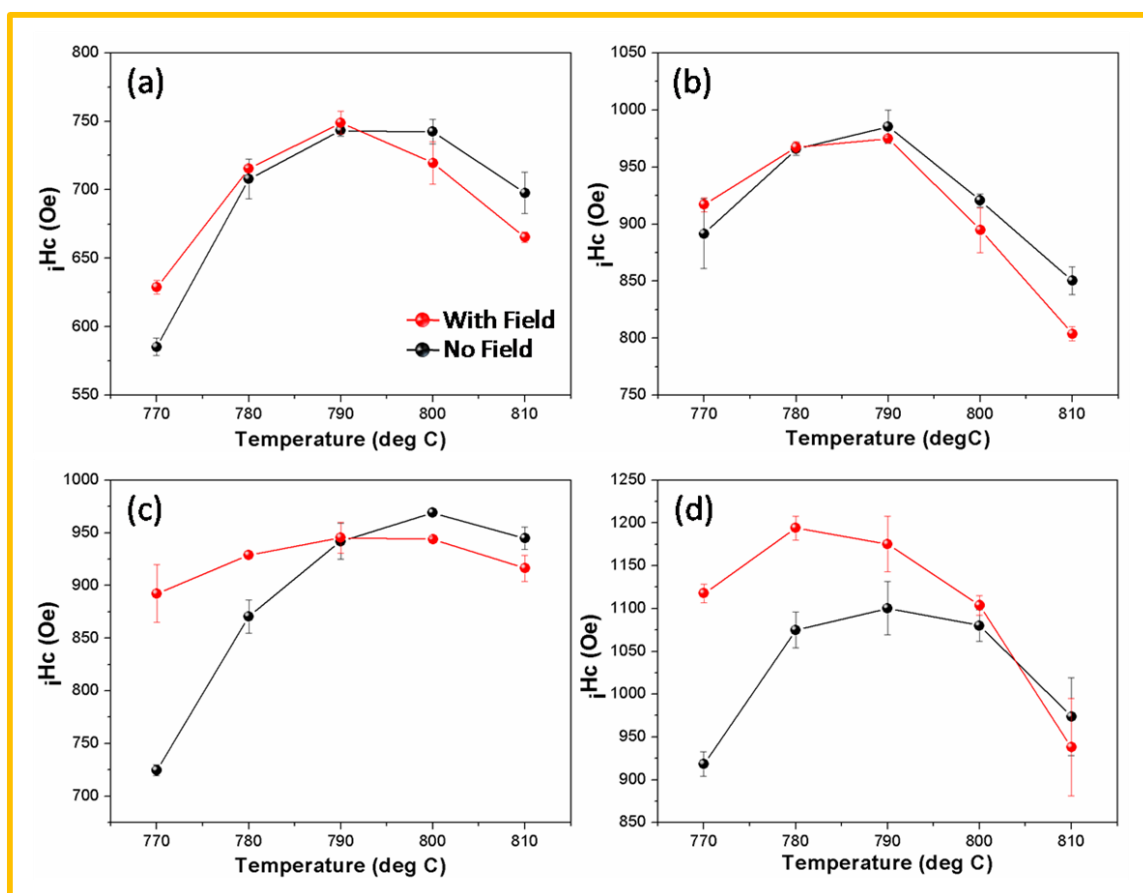
**Figure 49. Effect of magnetic field on the intrinsic coercivity of (a) sample 1, (b)
sample 2, (c) sample 3, and (d) sample 4.**
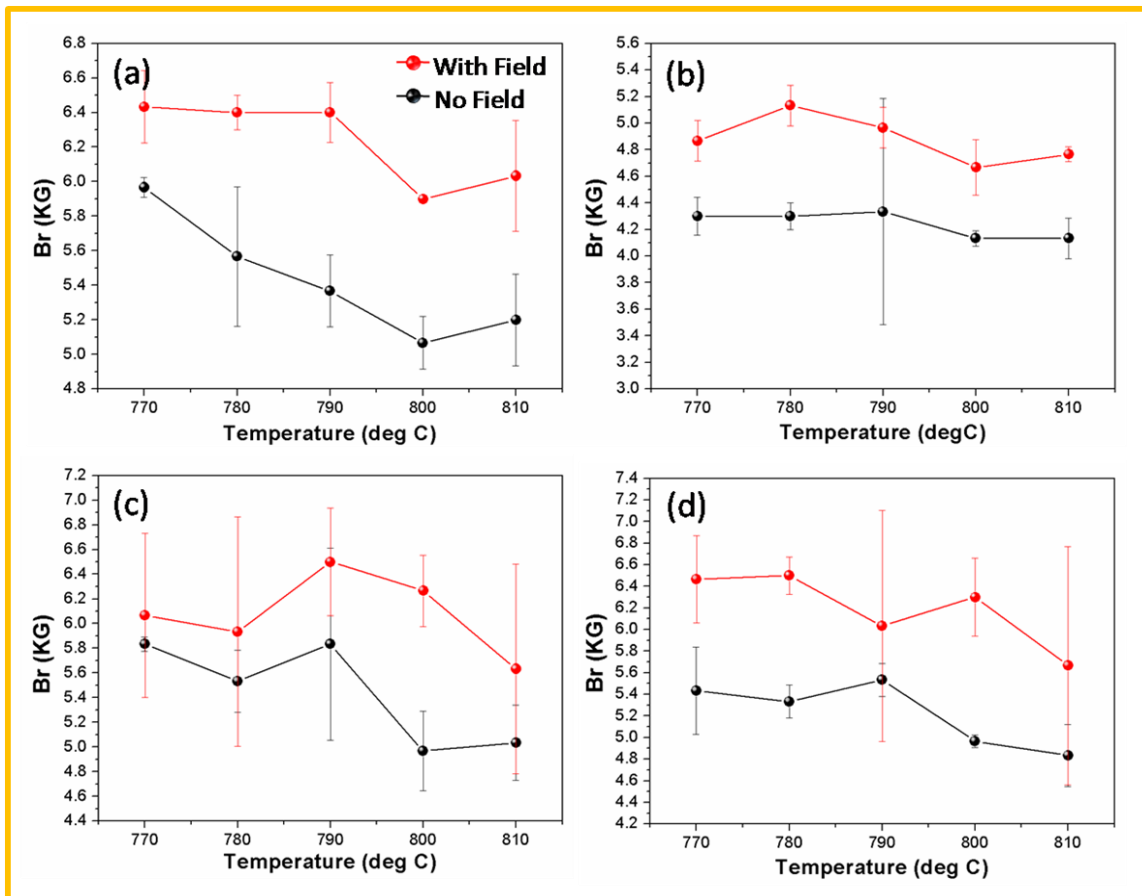
Figure 50. Effect of magnetic field on the remanence of (a) sample 1, (b) sample 2, (c) sample 3, and (d) sample 4.
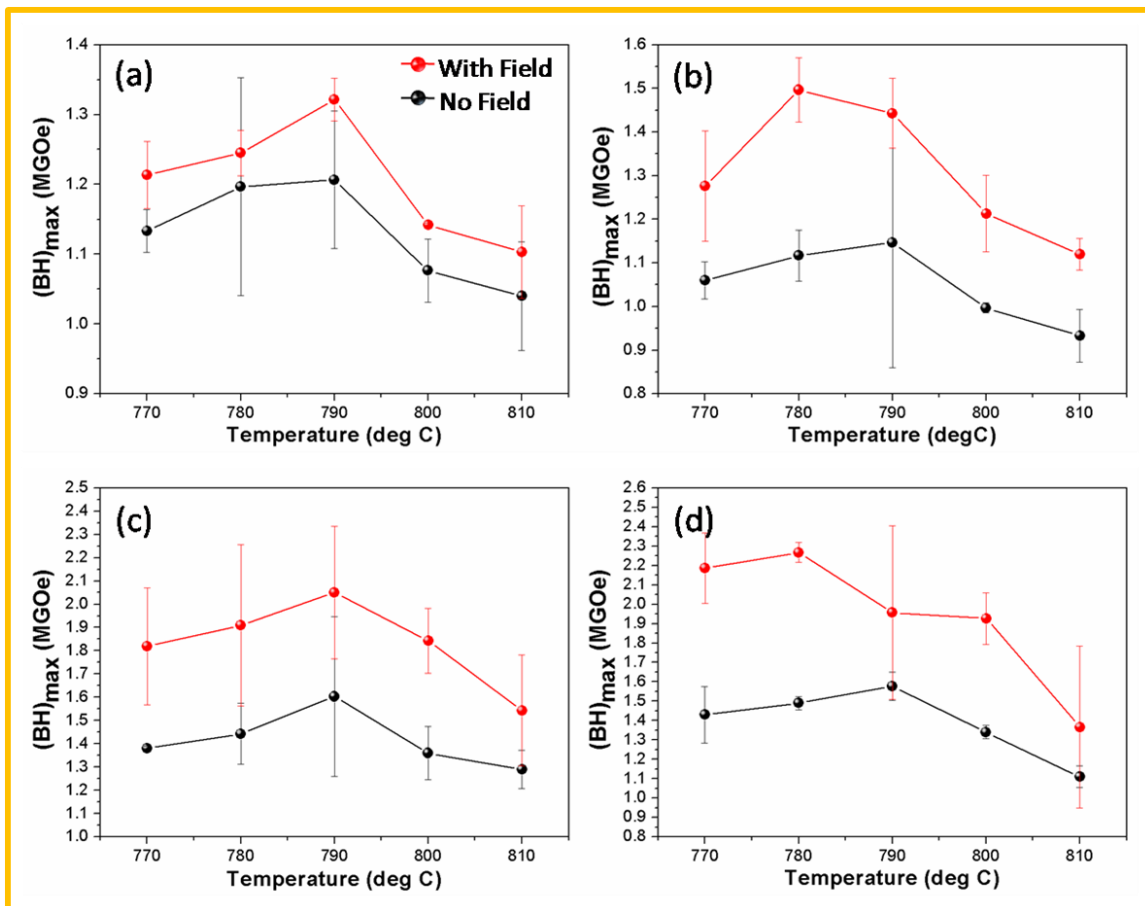
Figure 51. Effect of magnetic field on the energy product of (a) sample 1, (b) sample 2, (c) sample 3, and (d) sample 4.
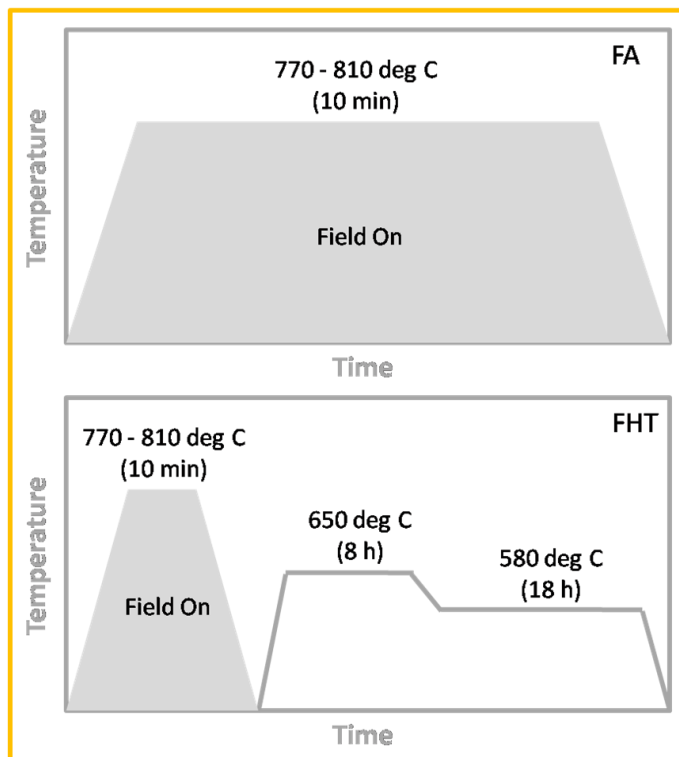
Figure 52. Schematic diagram of field annealing and full heat treatment process. FA indicates field annealing, FHT indicates full heat treatment.

We selected sample 3 and 4 for full heat treatment (FHT), since they have better magnetic properties. The heat treatment process is shown in Figure 52. As can be seen in Figure 53, sample 3 has a 30% improvement in coercivity, while sample 4 has a 15 to 30%. Remanence has no obvious change. Energy product has minor improvement. Figure 54 shows hysteresis loop of sample 4, a maximum coercivity of 1416 Oe can be obtained.

In summary, field annealing is an effective method to improve magnetic properties of Alnico alloys. The presence of magnetic field decreases optimal IHT temperature, and its effectiveness on magnetic properties varies with chemical composition and IHT temperature.
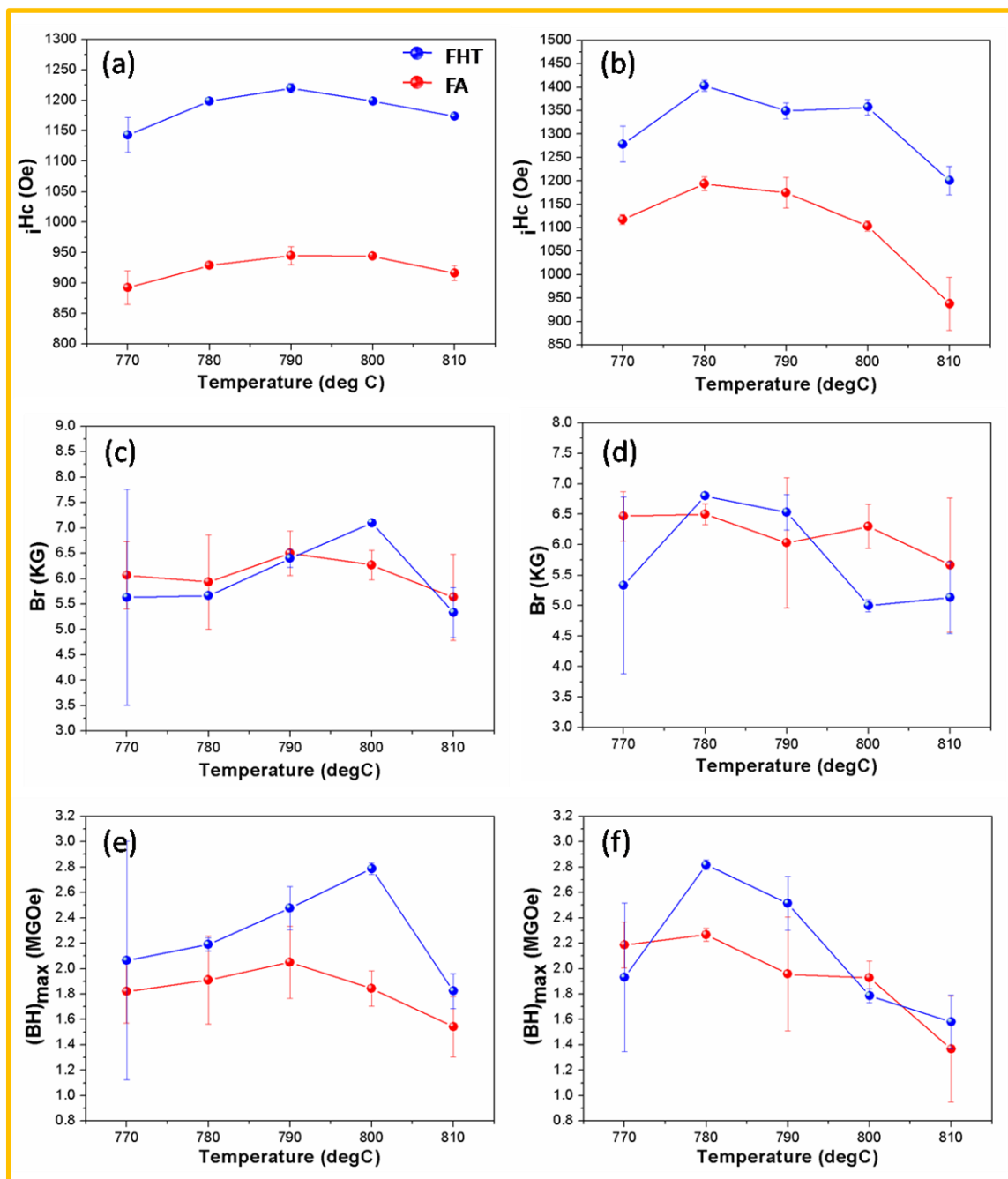
Figure 53. Magnetic properties of sample 3 and sample 4 after field annealing (FA) and full heat treatment (FHT). Coercivity of (a) sample 3 and (b) sample 4 vary with IHT temperature. Remanence of (c) sample 3 and (d) sample 4 vary with IHT temperature. Energy product of (e) sample 3 and (f) sample 4 vary with IHT temperature. (red lines indicate field annealing, blue lines indicate full heat treatment)
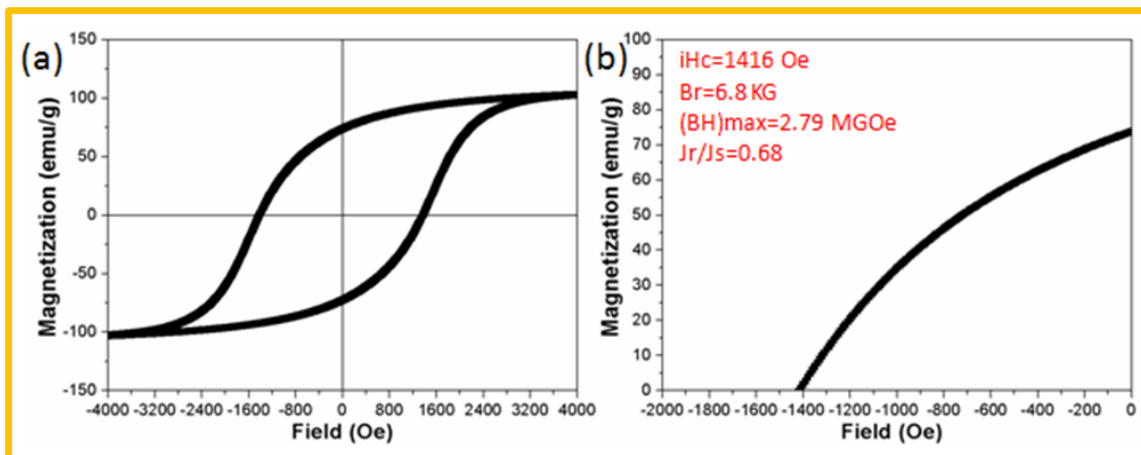
Figure 54. Hysteresis loop of sample 4 after FHT.

Chapter 8 Conclusion

In conclusion, we tried to improve magnetic properties of Alnico by controlling shape anisotropy and grain microstructure. For shape anisotropy, different alloy compositions and heat treatments were investigated. We found its coercivity is highly sensitive to isothermal heat treatment temperature and time. Co increase spinodal decomposition temperature while it is decreased by Ti. Although secondary and tertiary heat treatments further improve magnetic properties of Alnico while they are not sensitive to heat treatment temperature and time. It is because shape anisotropy has mainly been developed during isothermal heat treatment. For grain microstructure, we found that magnetic properties of melt-spun Alnico ribbons were controlled by wheel speed. Spinning speed at 20 mps yields optimal magnetic properties. We fabricated textured Alnico by setting up a simple casting system. However, its magnetic properties were not improved. Since a steep temperature gradient is not stable during casting process, resulting in a tilt of columnar crystals. In addition, the deleterious effects of γ phase and S may overshadow the benefit of texture.

We studied the effect of alloying additions on the avoidance of γ phase, and found 0 to 1 wt% Sn effectively suppress the formation of γ phase. It is likely that Sn is an α phase stabilizer or tend to decrease the temperature range where γ phase is stable. Ge has a similar effect. However, both of them have deleterious effects on magnetic properties. It is likely that they will ruin shape anisotropy or form impurity phases in Alnico.

We also examined the effect of field annealing on magnetic properties of Alnico. We found that the presence of magnetic field decreases IHT temperature. It is likely that a magnetic field promotes spinodal decomposition. Therefore, the optimal temperature is decreased. For the melt-spun Alnico 9 sample, the maximum coercivity of 1416 Oe can be obtained after FHT.

Chapter 9 Reference

[1] Wikipedia, "Lodestone." [Online]. Available:

https://en.wikipedia.org/wiki/Lodestone#cite_ref-15. [Accessed: 06-Mar-2016].

[2] 黎翔鳳 and 管仲, 管子校注, vol. 2. 中華書局, 2004.

[3] 吕不韦, 吕氏春秋, vol. 129. 艺术中国网, 1927.

[4] Baidu, "指南针." [Online]. Available:

http://baike.baidu.com/subview/4182/10985889.htm. [Accessed: 06-Mar-2016].

[5] 韩非子, "诸子集成," 上海上海书店出版社, 1986.

[6] 王充, 论衡, vol. 19. 艺术中国网, 2008.

[7] 王振铎, "司南，指南针与罗经盘," *中国社会科学院考古研究所. 科技考古论
丛 O*, vol. 5, 1989.

[8] 杨东晓, "传统'勺状'司南根本无法指南历史上真司南或是指南车," 2015.

[Online]. Available: http://news.ifeng.com/a/20150310/43308499_0.shtml.

[Accessed: 06-Mar-2016].

[9] gitam, "Hard Ferromagnetic." [Online]. Available:

http://www.gitam.edu/eresource/Engg_Phys/semester_2/magnetic/hard.htm.

[Accessed: 06-Mar-2016].

[10] T. Mishima, "Nickel-aluminum steel for permanent magnets," *Ohm*, vol. 19, p.

353, 1932.

[11] M. Tokushichi, "Magnet steel containing nickel and aluminium." Google Patents,

14-Jan-1936.

[12]   Wikipedia, "Alnico." [Online]. Available: https://en.wikipedia.org/wiki/Alnico.

        [Accessed: 08-Mar-2016].

[13]   E.-M. UK, "How Alnico Magnets are made," *Alnico Specialists*. [Online].

        Available: http://www.alnico-info.com/alnico_magnets_made.aspx. [Accessed:

        23-Feb-2016].

[14]   Dailymag, "What is the application of magnets?" [Online]. Available:

        http://www.cndailymag.com/use.htm. [Accessed: 06-Mar-2016].

[15]   F. Harvey, "Everything you need to know about the Paris climate summit and UN

        talks," *The Guardian*, 2015. [Online]. Available:

        http://www.theguardian.com/environment/2015/jun/02/everything-you-need-to-kn

        ow-about-the-paris-climate-summit-and-un-talks. [Accessed: 07-Mar-2016].

[16]   S. Scauzillo, "How much can electric cars impact climate change? New report says

        a lot." [Online]. Available:

        http://www.sgvtribune.com/environment-and-nature/20150929/how-much-can-ele

        ctric-cars-impact-climate-change-new-report-says-a-lot. [Accessed: 07-Mar-2016].

[17]   T. Schelmetic, "Are Hybrid Vehicle Manufacturers Shifting Gears Away from

        Rare Earth Elements?," *Thomasnet*, 2012. [Online]. Available:

        http://news.thomasnet.com/IMT/2012/12/11/are-hybrid-vehicle-manufacturers-shif

        ting-gears-away-from-rare-earth-elements. [Accessed: 07-Mar-2016].

[18]   Molycorp, "Advanced Vehicles." [Online]. Available:

http://www.molycorp.com/products/rare-earths-many-uses/advanced-vehicles/.

[Accessed: 07-Mar-2016].

[19]   Wikipedia, "Cerium(III)oxide." [Online]. Available:

https://en.wikipedia.org/wiki/Cerium(III)_oxide. [Accessed: 07-Mar-2016].

[20]   tasmanmetals, "Principal Uses of Rare Earth Elements." [Online]. Available:

http://www.tasmanmetals.com/s/PrincipalUses.asp. [Accessed: 07-Mar-2016].

[21]   S. Yan, "China is about to tighten its grip on rare earth minerals," *CNN Money*.

[Online]. Available:

http://money.cnn.com/2015/06/05/investing/molycorp-china-rare-earth-minerals/.

[Accessed: 07-Mar-2016].

[22]   Ames Laboratory, "Development of Radically Enhanced alnico Magnets (DREAM)

for Traction Drive Motors." .

[23]   M. Tokushichi, "Strong permanent magnet with cobalt." Google Patents,

14-Jan-1936.

[24]   K. Prange, "Alnico, the Miracle Metal," 2009. [Online]. Available:

http://www.premierguitar.com/articles/Alnico_the_Miracle_Metal. [Accessed:

21-Feb-2016].

[25]   A. S. Rao and D. Ph, "Alnico Permanent Magnets," vol. 62, no. 1949, pp. 373–383,

1959.

[26]   E. R. Cronk, "Recent Developments in High-Energy Alnico Alloys," *J. Appl.

Phys.*, vol. 37, no. 3, p. 1097, 1966.

[27] J. E. Gould, "Magnets with columnar crystallization," *Cobalt & Cobalt Abstr*, vol. 23, pp. 82–87, 1964.

[28] M. McCaig, "Recent developments in permanent magnetism," *J. Appl. Phys.*, vol. 35, no. 3, pp. 958–965, 1964.

[29] A. Palasyuk, E. Blomberg, R. Prozorov, L. Yue, M. J. Kramer, R. W. McCallum, I. E. Anderson, and S. Constantinides, "Advances in characterization of non-rare-earth permanent magnets: Exploring commercial alnico grades 5-7 and 9," *Jom*, vol. 65, no. 7, pp. 862–869, 2013.

[30] L. Zhou, M. K. Miller, P. Lu, L. Ke, R. Skomski, H. Dillon, Q. Xing, A. Palasyuk, M. R. McCartney, D. J. Smith, S. Constantinides, R. W. McCallum, I. E. Anderson, V. Antropov, and M. J. Kramer, "Architecture and magnetism of alnico," *Acta Mater.*, vol. 74, pp. 224–233, 2014.

[31] W. Tang, L. Zhou, A. G. Kassen, A. Palasyuk, E. M. White, K. W. Dennis, M. J. Kramer, R. W. McCallum, and I. E. Anderson, "New alnico magnets fabricated from pre-alloyed gas-atomized powder through diverse consolidation techniques," *Magn. IEEE Trans.*, vol. 51, no. 11, pp. 1–3, 2015.

[32] I. E. Anderson, A. G. Kassen, E. M. H. White, L. Zhou, W. Tang, A. Palasyuk, K. W. Dennis, R. W. McCallum, and M. J. Kramer, "Novel pre-alloyed powder processing of modified alnico 8: Correlation of microstructure and magnetic properties," *J. Appl. Phys.*, vol. 117, no. 17, p. 17D138, 2015.

[33] Magnet Energy Corp, "PM history." [Online]. Available:

http://www.magnetnrg.com/pm-history.html. [Accessed: 07-Mar-2016].

[34] Y. Iwama and M. Takeuchi, "Spinodal Decomposition in Alnico 8 Magnet Alloy," *Trans. J I M*, vol. 15. pp. 371–377, 1974.

[35] R. W. Balluffi, S. Allen, and W. C. Carter, *Kinetics of materials*. John Wiley & Sons, 2005.

[36] D. A. Porter, K. E. Easterling, and M. Sherif, *Phase Transformations in Metals and Alloys, (Revised Reprint)*. CRC press, 2009.

[37] J. J. De Jong, J. M. G. Smeets, and H. B. Haanstra, "Some results of an electron microscopical study of the metallographic structure of two alloys for permanent magnets (Ticonal G and Ticonal X)," *J. Appl. Phys.*, vol. 29, no. 3, pp. 297–298, 1958.

[38] G. Marcon, R. Peffen, and H. Lemaire, "A contribution to the study of Alnico 5 thermal treatment in magnetic field," *Magn. IEEE Trans.*, vol. 14, no. 5, pp. 688–689, 1978.

[39] G. Begin and A. Dube, "Constitutional , morphological and magnetic properties of Alnico alloys," vol. 7, no. 1, pp. 35–39.

[40] Y. B. Kim, S. A. Song, and T. K. Kim, "Effects of the heat treatment on the microstructures and magnetic properties in Alnico 5," *Magn. IEEE Trans.*, vol. 23, no. 4, pp. 1952–1955, 1987.

[41] H. M. Dillon, "Effects of heat treatment and processing modifications on microstructure in alnico 8H permanent magnet alloys for high temperature

applications," 2014.

[42]   A. Hoffmann and H. StÄblein, "Investigations of high-coercivity alnico alloys," *Magn. IEEE Trans.*, vol. 6, no. 2, pp. 225–230, 1970.

[43]   W. G. Chu, W. D. Fei, X. H. Li, D. Z. Yang, and J. L. Wang, "Evolution of Fe-Co rich particles in Alnico 8 alloy thermomagnetically treated at 800C," *Mater. Sci. Technol.*, vol. 16, no. February, pp. 1023–1028, 2000.

[44]   B. G. Livshitz, B. A. Samarin, and V. S. Shubakov, "Features of the thermal magnetic treatment of ticonal 2000 type high-coercivity alloys," *Magn. IEEE Trans.*, vol. 6, no. 2, pp. 242–245, 1970.

[45]   C. A. Julien and F. G. Jones, "Alpha‑Sub‑Gamma Phase in Alnico 8 Alloys," *J. Appl. Phys.*, vol. 36, no. 3, pp. 1173–1174, 1965.

[46]   R. C. O'handley, *Modern magnetic materials: principles and applications*, vol. 830622677. Wiley New York, 2000.

[47]   T. Liu, W. Li, M. Zhu, Z. Guo, and Y. Li, "Effect of Co on the thermal stability and magnetic properties of AlNiCo 8 alloys," *J. Appl. Phys.*, vol. 115, no. 17, pp. 34–37, 2014.

[48]   Y. Iwama, M. Inagaki, and T. Miyamoto, "Effects of Titanium in Alnico 8-Type Magnet Alloys," *Trans. Japan Inst. Met.*, vol. 11, no. 4, pp. 268–274, 1970.

[49]   M. Takeuchi and Y. Iwama, "Effects of Titanium upon Magnetic Anisotropy and Coercivity in Alnico Magnet Alloys," *Trans. Japan Inst. Met.*, vol. 17, no. 8, pp. 489–496, 1976.

[50] S. Szymura and S. Golba, "The influence of Niobium on the magnetic properties of the columnar Alnico 5 permanent magnets," *J. Magn. Magn. Mater.*, vol. 24, no. 3, pp. 285–287, 1981.

[51] M. Sugiyama and K. Shida, "The effect of the addition of niobium on sintered Alnico magnet properties.," *Trans. Japan Inst. Met.*, vol. 3, no. 2, 1962.

[52] B. D. Cullity and C. D. Graham, *Introduction to magnetic materials*. John Wiley & Sons, 2011.

[53] M. Durand-Charre, C. Bronner, and J.-P. Lagarde, "Relation between magnetic properties and crystallographic texture of columnar Alnico 8 permanent magnets," *Magn. IEEE Trans.*, vol. 14, no. 5, pp. 797–799, 1978.

[54] N. Makino and Y. Kimura, "Effect of duplex addition of S and Te in the columnar alnico magnet alloys containing Ti," *Magn. IEEE Trans.*, vol. 6, no. 2, pp. 302–303, 1970.

[55] W. Wright and A. Thomas, "Influence de aluminum et du titane sur la structure de solidification des alliages magnetiques du tupe Alnico," *Cobalt*, vol. 13, pp. 24–28, 1961.

[56] A. I. Luteijn and K. J. de Vos, "Philips Res. Rept. 11, 489 (1956); AJJ Koch," in *MG van der Steeg, and KJ de Vos, Proc. AIEE Conf. Magnetism Magnetic Materials, Boston*, 1956, p. 173.

[57] N. Makino and Y. Kimura, "Techniques to achieve texture in permanent magnet alloy systems," *J. Appl. Phys.*, vol. 36, no. 3, pp. 1185–1190, 1965.

[58]   Wikipedia, "Melt spinning." [Online]. Available:

https://en.wikipedia.org/wiki/Melt_spinning. [Accessed: 09-Mar-2016].

[59]   W. D. Callister and D. G. Rethwisch, *Materials science and engineering: an introduction*, vol. 7. Wiley New York, 2007.

[60]   S. Dris, "Magnetic Hysteresis." [Online]. Available:

http://chemwiki.ucdavis.edu/Core/Materials_Science/Magnetic_Properties/Magnet

ic_Hysteresis. [Accessed: 07-Mar-2016].

[61]   B. Butrow and C. Clark, "X-ray Powder Diffraction (XRD)." [Online]. Available:

http://serc.carleton.edu/research_education/geochemsheets/techniques/XRD.html.

[Accessed: 07-Mar-2016].

[62]   Wikipedia, "X-ray crystallography." [Online]. Available:

https://en.wikipedia.org/wiki/X-ray_crystallography. [Accessed: 07-Mar-2016].

[63]   Wikipedia, "Bragg's law." .

[64]   Wikipedia, "Metallography." .

[65]   Wikipedia, "Microscopy." [Online]. Available:

https://en.wikipedia.org/wiki/Microscopy. [Accessed: 08-Mar-2016].

[66]   Wikipedia, "Optical microscope." [Online]. Available:

https://en.wikipedia.org/wiki/Optical_microscope. [Accessed: 08-Mar-2016].

[67]   and E. G. P. K.I.Vlaskina,N.F.Kartashova, "Heat treatment of Ticonal Alloys," *Metalloved. i Termicheskaya Obrab. Met.*, vol. 2, pp. 29–32, 1970.

[68]   J. W. Cahn, "On spinodal decomposition in cubic crystals," *Acta Metall.*, vol. 10,

no. 3, pp. 179–183, 1962.

[69] J. W. Cahn, "Magnetic aging of spinodal alloys," *J. Appl. Phys.*, vol. 34, no. 12, pp. 3581–3586, 1963.

[70] J. W. Cahn, "The later stages of spinodal decomposition and the beginnings of particle coarsening," *Acta Metall.*, vol. 14, no. 12, pp. 1685–1692, 1966.

[71] R. Ramesh, G. Thomas, and B. M. Ma, "Magnetization reversal in nucleation controlled magnets. II. Effect of grain size and size distribution on intrinsic coercivity of Fe‑Nd‑B magnets," *J. Appl. Phys.*, vol. 64, no. 11, pp. 6416–6423, 1988.

[72] K. Hono and H. Sepehri-Amin, "Strategy for high-coercivity Nd-Fe-B magnets," *Scr. Mater.*, vol. 67, no. 6, pp. 530–535, 2012.